Journal of Medicinal Chemistry

pubs.acs.org/jmc

Article

Bis-6-amidino-benzothiazole Derivative that Cures Experimental Stage 1 African Trypanosomiasis with a Single Dose

Livio Racané,* Lucija Ptiček, Sanja Kostrun, Silvana Raić-Malić, Martin Craig Taylor, Michael Delves, Sam Alsford, Francisco Olmo, Amanda Fortes Francisco, and John M. Kelly*

Cite This: https://doi.org/10.1021/acs.jmedchem.3c01051

Read Online

ACCESS | Metrics & More | Article Recommendations | Supporting Information

ABSTRACT: We designed and synthesized a series of symmetric bis-6-amidino-benzothiazole derivatives with aliphatic central units and evaluated their efficacy against bloodstream forms of the African trypanosome *Trypanosoma brucei*. Of these, a dicationic benzothiazole compound (**9a**) exhibited sub-nanomolar in vitro potency with remarkable selectivity over mammalian cells (>26,000-fold). Unsubstituted 5-amidine groups and a cyclohexyl spacer were the crucial determinants of trypanocidal activity. In all cases, mice treated with a single dose of 20 mg kg^{-1} were cured of stage 1 trypanosomiasis. The compound displayed a favorable in vitro ADME profile, with the exception of low membrane permeability. However, we found evidence that uptake by *T. brucei* is mediated by endocytosis, a process that results in lysosomal sequestration. The compound was also active in low nanomolar concentrations against cultured asexual forms of the malaria parasite *Plasmodium falciparum*. Therefore, **9a** has exquisite cross-species efficacy and represents a lead compound with considerable therapeutic potential.

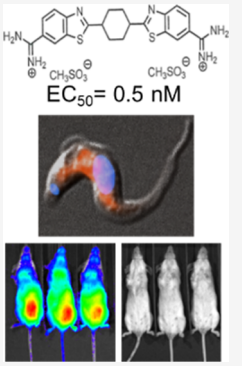

1. INTRODUCTION

African trypanosomiasis is caused by infection with tsetse fly-transmitted parasites of the *Trypanosoma brucei* species complex and has been a major medical and veterinary problem throughout sub-Saharan Africa. Recently, a combination of public health measures has reduced the number of those infected to below 1000 per year[1] although there remains the potential for large epidemic outbreaks. Livestock infections continue to impose a substantial burden on the rural poor, with estimates of more than $4.5 billion in economic losses.[2] Within the mammalian host, *T. brucei* is entirely extracellular, initially in the blood and interstitial spaces, with a process of antigenic variation protecting the parasite against elimination by the humoral immune system. The disease transitions to stage 2 when parasites access the central nervous system (CNS), leading to meningoencephalitis and a range of neurological conditions that give rise to the classical "sleeping sickness" symptoms. In the absence of treatment, stage 2 infections are inevitably fatal. More recently, the role of parasites located in other tissues, particularly in skin and adipose reservoirs, has also attracted attention in terms of persistence, pathology, and transmission.[3,4]

Therapies for trypanosomiasis have been unsatisfactory because of toxicity, limited efficacy, long treatment regimens, and the requirement for parenteral administration.[5] For example, although pentamidine is usually effective during the initial hemolymphatic stage of *Trypanosoma brucei gambiense* infections, it cannot cross the blood−brain barrier (BBB) and is non-curative against stage 2 disease.[6] The arsenical drug melarsoprol, which was used to treat stage 2 infections, has severe side effects, including reactive encephalopathy, which kills up to 10% of patients, and resistance has become an issue.[7] For *T. b. gambiense* infections, melarsoprol has now been superceded by nifurtimox−eflornithine combination therapy,[8] although treatment length remains an issue. A major recent advance has been the roll-out of the heterocyclic drug fexinidazole as the first oral treatment for trypanosomiasis.[9,10] The recommended regimen is 10 daily doses under medical supervision.[1] Despite being an important step forward, relapses and toxicity associated with fexinidazole treatment have been reported.[9] For livestock infections, the most commonly used drugs are diminazene and isometamidium.[11] However, these do not cross the BBB, and their widespread prophylactic use has raised concerns about the development of resistance.[12]

Further attempts to develop improved trypanocidal agents have included studies on benzazoles[13−17] and their amidine derivatives,[18−23] where enhancement of activity has been achieved through optimization of physicochemical parameters and ADME properties. The introduction of nitrogen atoms into the aromatic rings can change the lipophilicity and polarity of the resulting aza analogues, enabling them to cross the BBB.[24,25] Some benzimidazole[26−28] and benzothia-

Received: June 12, 2023

Scheme 1. Synthesis of Bis-6-amidino-substituted-2-(alkyl/alkenyl) Benzothiazoles 3a−10a, 3b−10b and 3c−10c

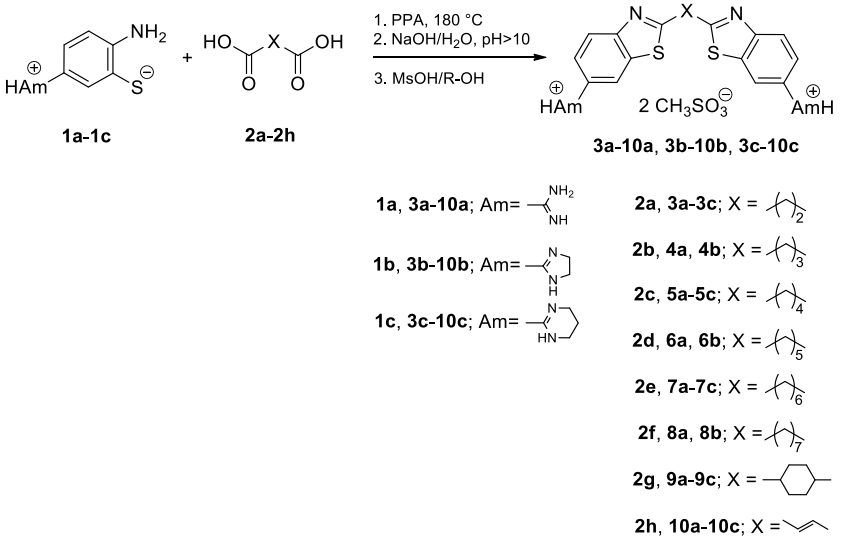

zole[29−32] derivatives have been shown to have potent anti-trypanosomatid activity. As an example, 6-(trifluoromethyl)-benzothiazole, which contains a cyclopropanecarboxamide moiety, was identified as a lead with improved antiparasitic activity and promising in vivo efficacy.[33] In the 6-amidino-2-arylbenzothiazole series, the effects of both the amidino substituent and the type of linker between benzazole and the 1,2,3-triazole scaffolds were crucial determinants for anti-trypanosomal potency.[34−37] Replacement of the amidine group with less basic and ionizable nitrogen-containing moieties failed to improve anti-trypanosomal activity and membrane permeability.[35] Furthermore, within symmetric bis-benzimidazoles, imidazoline and 1,4-bis(oxymethylene)phenyl were favorable for strong antiprotozoal effects.[36] In continuation of studies on the potential of aromatic benzazole amidines as anti-trypanosomal agents,[34−37] we have now designed and synthesized head-to-head bis-6-amidino-benzothiazoles by the fusion of two benzothiazole scaffolds through aliphatic central units constituted by alkyl, cycloalkyl, or alkenyl spacers (Scheme 1, Table 1). One of these compounds, **9a**, displays sub-nanomolar activity against bloodstream form *T. brucei* and can cure experimental stage 1 infections with a single dose. In addition, **9a** has potency against *Plasmodium falciparum* merozoites, the replicating asexual blood-stage forms of the human malaria parasite.

2. RESULTS

2.1. Chemistry. To explore the biological activity of unsubstituted and two cyclic 6-amidino-substituted bis-benzothiazoles, we synthesized 21 bis-6-amidino-benzothiazoles linked through aliphatic units, as presented in Scheme 1. We have developed robust methods for the preparation of mono- and bis-6-amidino-2-aryl/heteroaryl-benzothiazole derivatives by a condensation reaction of 5-amidino-, 5-imidazolinyl- and 5-pyrimidinyl-substituted 2-aminothiophenols with carboxylic acids in polyphosphoric acid (PPA).[38−40] This method was applied for the condensation of 2-aminothiophenols with carboxylic acids, leading to cyclization and the formation of a benzothiazole ring.[41]

To assess the influence of the type of amidino-substituents introduced at C-6 of the benzothiazole moiety, we prepared unsubstituted 2-imidazolinyl and 2-pyrimidinyl 2-aminothiophenols from 6-cyanobenzothiazoles by the Pinner reaction, as previously reported.[42,43] Reaction of zwitterionic forms of 5-amidino-substituted 2-aminothiophenols (**1a−1c**) with aliphatic dicarboxylic acids (**2a−2f**), *trans*-1,4-cyclohexane dicarboxylic acid (**2g**), and fumaric acid (**2h**) resulted in bis-6-amidino-benzothiazole derivatives **3a−10a**, **3b−10b**, and **3c−10c**. Since methanesulfonates of amidine derivatives of 2-phenylbenzothiazoles are more stable and soluble in water than chlorides,[44] target compounds were isolated as methanesulfonates by an additional acid−base reaction.

2.2. In Vitro Evaluation of Anti-Trypanosomal Activity. In vitro activity against bloodstream form *T. brucei* was established for the 6-amidinobenzotiazole derivatives **3a−10c**, with fexinidazole as the reference drug (Table 1). Cytotoxicity was assessed using the L6 rat myoblast cell line. Most of the tested compounds were more potent than fexinidazole, with EC_{50} values against *T. brucei* ranging from 0.51 nM to 5.39 μM. There was a relationship between the type of amidino moiety and anti-trypanosomal activity. With the exception of **7a−7c**, trypanocidal activity decreased in the following order: unsubstituted amidine > pyrimidine > imidazoline. The nature of the spacer between the two benzothiazole scaffolds also influenced activity. The cyclohexyl unit in **9a−9c** had the most pronounced impact, with the bis-benzothiazole **9a**, which contains an unsubstituted amidino moiety, displaying remarkable potency (EC_{50} = 0.51 nM). Compounds **10a−10c**, which have conformationally constrained ethenyl spacers, had better activity than the corresponding **3a−3c** derivatives, which have a conformationally unrestricted ethyl spacer. In the compounds with conformationally unrestricted alkyl chains of different lengths (**3−8**), a unit size of 4 was generally optimal, although the highly active derivative **7c** did not conform to this trend. Thus, among bis-benzothiazoles containing a central alkyl unit, **5a**, **6a** (butyl and pentyl chains, respectively), and **7c** (hexyl chain) had the most potent trypanocidal activities. Importantly, all evaluated compounds exhibited considerable selectivity over mammalian cells, particularly the unsubstituted diamidine **9a** (SI = 26,300).

To further evaluate compound **9a**, we examined dose- and time-dependent growth inhibition of *T. brucei*. This revealed that in the low nanomolar range, inhibition was relatively slow-

https://doi.org/10.1021/acs.jmedchem.3c01051
J. Med. Chem. XXXX, XXX, XXX−XXX

Table 1. Anti-Trypanosomal Activity[a] of Bis-6-amidino-benzothiazoles 3a−10c against Cultured Bloodstream Form *T. brucei* (Experimental Section)

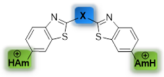

3a-10a, 3b-10b, 3c-10c

Compound	X	Am	*T. brucei*		L6 cells	SI[b]
			EC_{50} (μM)	EC_{90} (μM)	EC_{50} (μM)	EC_{50} (L6/Tb)
3a			0.25 ± 0.03	0.40 ± 0.02	>170	>680
3b			3.64 ± 0.13	7.82 ± 0.13	80.6 ± 2.6	22
3c			2.38 ± 0.07	3.48 ± 0.06	>140	>59
4a			0.34 ± 0.02	0.75 ± 0.01	>160	>470
4b			5.39 ± 0.23	9.01 ± 1.39	>150	>28
5a			0.063 ± 0.001	0.131 ± 0.003	134 ± 2	2,100
5b			1.14 ± 0.10	1.87 ± 0.20	93.0 ± 6.6	82
5c			0.19 ± 0.03	0.31 ± 0.01	>130	>680
6a			0.098 ± 0.002	0.145 ± 0.002	114 ± 9	1,200
6b			1.56 ± 0.03	2.11 ± 0.07	93.5 ± 5.8	60
7a			0.89 ± 0.08	1.52 ± 0.06	42.5 ± 3.5	48
7b			0.82 ± 0.10	1.88 ± 0.19	10.9 ± 4.7	13
7c			0.028 ± 0.001	0.056 ± 0.001	>130	>4,600
8a			0.74 ± 0.03	1.39 ± 0.02	13.9 ± 1.4	18
8b			1.49 ± 0.19	2.52 ± 0.04	6.85 ± 1.07	4.6
9a			0.00051± 0.00003	0.00115± 0.00005	13.4 ± 2.4	26,300
9b			0.24 ± 0.03	0.49 ± 0.04	4.15 ± 0.74	17
9c			0.021 ± 0.002	0.031 ± 0.001	>130	>6,200
10a			0.012 ± 0.001	0.022 ± 0.006	2.48 ± 0.45	210
10b			0.19 ± 0.04	0.68 ± 0.07	4.10 ± 0.83	22
10c			0.10 ± 0.01	0.16 ± 0.02	51.8 ± 1.3	520
FEX			2.40 ± 0.18	4.51 ± 0.57		

[a]In vitro activity against bloodstream form *T. brucei* was determined using microtiter plate assays (Experimental Section). Values are expressed as the concentration that inhibited growth by 50% (EC_{50}) and 90% (EC_{90}). The data are the mean of triplicate experiments ± SEM. [b]Selectivity index, SI = [EC_{50} L6 cells]/[EC_{50} *T. brucei*]. FEX = fexinidazole.

acting, taking up to 2 days to become apparent (Figure 1). Thereafter, activity was progressive, so that from day 6, concentrations as low as 0.3 nM had a noticeable inhibitory impact. *T. brucei* were also exposed to a range of drug concentrations for 3 days, transferred into compound-free medium, and then monitored for 12 days. Parasites exposed to 1.2 nM and above did not recover, and treatment resulted in 100% lethality. Thus, **9a** appears to have a cytotoxic rather than a cytostatic mode of action.

2.3. In Silico and In Vitro Profiling of ADME Properties. The ADME properties of the bis-6-amidino-benzothiazole derivatives **3a−10c** were first evaluated in silico (Table 2, Experimental Section). Compounds were predicted to have moderate lipophilicity (with log *P* in the range from 2.1 to 4.2) and to be strong bases due to the presence of the amidine moieties. Solubility was calculated to decrease with the length of the linker, with compounds containing linkers of up to 3 carbon atoms expected to have moderate solubility. The permeability of all compounds, particularly the unsubstituted diamidines, was calculated to be low with a slight enhancement due to the increased lipophilicity and introduction of cyclic amidine structures. Pe (Caco-2) values are considered reliable predictors of intestinal permeability from the duodenum to the colon.[45] Five-membered amidines were predicted to have the best permeability within the current compound set (Figure 2). The free fraction was assessed to be between 3 and 4%.

Permeability and metabolic stability in mouse liver microsomes were experimentally determined for the compound **9a**. These properties significantly affect the oral bioavailability of drugs and are routinely screened in the early drug discovery phases.[46] The Madin−Darby canine kidney cell line, which overexpresses the human multidrug-resistance gene (*MDCKII-hMDR1*) and is frequently used to study bi-directional transport of compounds,[47] was used in this study (Experimental Section). Apparent permeability (P_{app}) values were determined from the amount permeated through the MDCKII-hMDR1 cell monolayer in both the apical-basolateral (AB) and basolateral-apical (BA) directions (Table 3).

Compound **9a** was characterized as having low permeability, with AB values below 0.1×10^{-6} cm s^{-1}. The P_{app} value in the BA direction was somewhat higher at 0.4×10^{-6} cm s^{-1}. An efflux ratio for **9a** could not be determined. Incubation with mouse liver microsomes suggested that **9a** is a metabolically stable compound which exhibits low clearance values (<30% liver blood flow, LBF) with $t_{1/2}$ > 60 min, as summarized in Table 3.

2.4. Evaluation of In Vivo Activity. To assess the in vivo efficacy of compound **9a**, we used an experimental murine model infected with a highly bioluminescent *T. brucei* strain that constitutively expresses a red-shifted luciferase[48] (Experimental Section). In untreated BALB/c mice, this produces a lethal outcome 20−30 days post-infection, although in accordance with welfare regulations, animals are euthanized before they reach the terminal stage. Initially, infected mice were treated with a range of i.p. doses (once daily for 4 days) and monitored regularly by in vivo imaging. At the experimental endpoint, ex vivo imaging was used to further examine organs and tissues (Figure 3). No signs of toxicity were observed (e.g., piloerection, hunching, shaking, or lack of activity) under any of the dosing or administration regimens, although mice treated for 4 days at 20 mg kg^{-1} by the i.p. route exhibited a minor (<10%), but transient weight loss. All mice treated with 5 mg kg^{-1} and above were assessed as cured in the absence of relapse. Some curative outcomes were achieved with doses down to 0.25 mg kg^{-1} (Figure 3, Table 4). In line

https://doi.org/10.1021/acs.jmedchem.3c01051
J. Med. Chem. XXXX, XXX, XXX−XXX

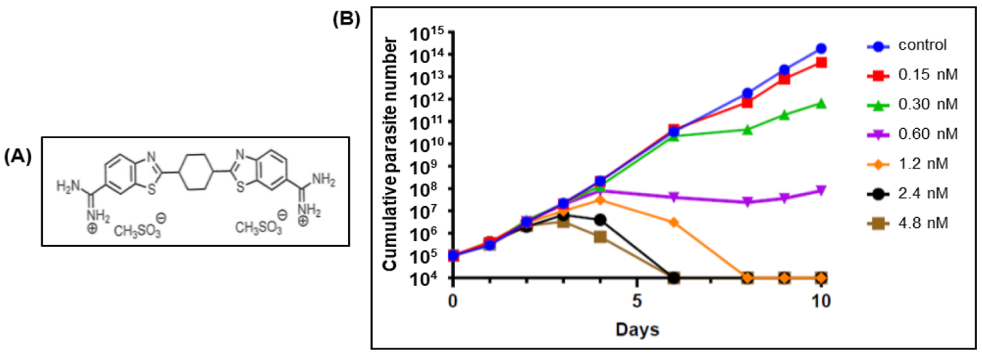

Figure 1. In vitro activity of compound **9a** against bloodstream form *T. brucei*. (A) Structure of compound **9a**. (B) Activity against cultured trypanosomes. *T. brucei* were seeded into culture flasks at 10^5 mL^{-1} (5 mL volumes) and incubated in the presence of a range of **9a** concentrations (Experimental Section). After 24 h, parasites were sub-cultured back to 10^5 mL^{-1} and incubated for a further 24 h in the continued presence of the test compound. This continued until day 10. Parasite growth is expressed as the cumulative parasite number.

Table 2. Calculated PhysChem and ADME Parameters for Synthesized Compounds[a]

compd	log *P*	log *D* (pH = 7.40)	HBD	HBA	TPSA	MW	pK_a	% PPB	Pe (Caco-2) 10^{-6} cm/s
3a	2.06	−0.92	6	6	182	380.49	10.55	93.35	0.21
3b	2.60	−0.37	2	6	131	432.57	9.79	96.61	1.35
3c	3.10	0.10	2	6	131	460.62	11.76	97.43	1.32
4a	2.18	−0.80	6	6	182	394.52	10.61	93.40	0.18
4b	2.76	−0.21	2	6	131	446.59	9.81	96.32	1.52
5a	2.63	−0.35	6	6	182	408.55	10.63	93.76	0.16
5b	3.08	0.11	2	6	131	460.62	9.82	97.10	2.08
5c	3.63	0.63	2	6	131	488.67	11.85	97.56	2.24
6a	2.94	−0.04	6	6	182	422.57	10.64	94.93	0.16
6b	3.33	0.36	2	6	131	474.65	9.82	97.30	2.68
7a	3.27	0.29	6	6	182	436.60	10.64	94.54	0.17
7b	3.66	0.69	2	6	131	488.67	9.82	97.33	3.79
7c	4.23	1.23	2	6	131	516.73	11.86	97.73	4.20
8a	3.48	0.50	6	6	182	450.63	10.65	96.28	0.19
8b	4.16	1.19	2	6	131	502.70	9.82	97.78	6.47
9a	2.70	−0.28	6	6	182	434.58	10.61	95.36	0.16
9b	3.35	0.38	2	6	131	486.66	9.79	98.43	2.85
9c	3.9	0.90	2	6	131	514.71	11.82	98.73	2.96
10a	2.00	−0.97	6	6	182	378.48	10.37	93.62	0.23
10b	2.69	−0.26	2	6	131	430.55	9.73	96.47	1.62
10c	3.29	0.29	2	6	131	458.60	11.59	97.21	1.61

[a]HBD—hydrogen bond donors; HBA—hydrogen bond acceptors; TPSA—total polar surface area; MW—molecular weight; % PPB—percentage of plasma protein binding; and Pe (Caco-2)—permeability in Caco-2 cells.

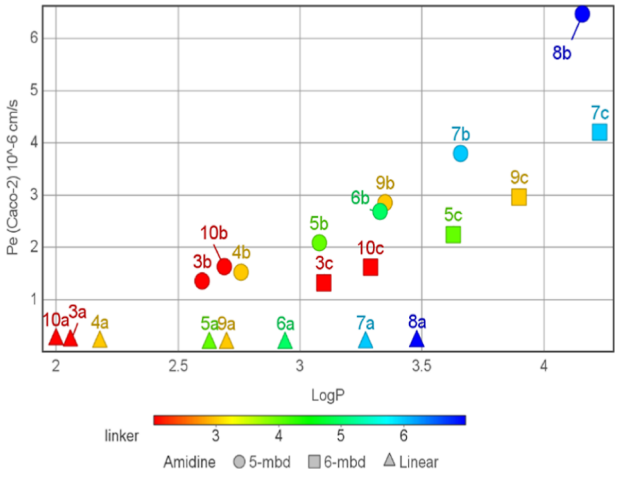

Figure 2. Predicted permeability and lipophilicity for the prepared compounds.

with the slow-acting and progressive nature of in vitro activity (Figure 1B), and the low compound clearance values (Table 3), whole-body bioluminescence flux continued to decrease up to a week after the cessation of treatment before reaching background levels (Figure 3B). Oral dosing was less effective, with a cure rate of 20% (1/5) at 20 mg kg^{-1} (Figure 3A). When the efficacy of single i.p. dosing 4 days post-infection was assessed (Figure 4), treatment at 20 mg kg^{-1} resulted in a 100% (10/10) cure rate. Again, parasite killing was still apparent between 3 and 7 days post-treatment, as evidenced by the continued reduction in the bioluminescence signal (Figure 4B). At lower doses, down to 1 mg kg^{-1}, some curative outcomes were observed (Table 4). To investigate activity against stage 2 infections, treatment was delayed until day 13, by which point, in this model, parasites have accessed the CNS.[48] No cures were achieved following 3 daily doses with 10 or 20 mg kg^{-1}, although the total mouse burden was initially reduced by >99.99% (Figure S1). This was followed by a small infection relapse, often focused in the cranial region.

https://doi.org/10.1021/acs.jmedchem.3c01051
J. Med. Chem. XXXX, XXX, XXX−XXX

Table 3. Apparent Permeability (P_{app}) of 9a in a MDCKII-hMDR1 Cell Assay from Apical-to-Basolateral (AB) and Basolateral-to-Apical (BA) Sides and Metabolic Stability Parameters in Mouse Liver Microsomes

compound	AB P_{app} ($\times 10^6$ cm/s)	BA P_{app} ($\times 10^6$ cm/s)	efflux ratio (BA/AB)	$t_{1/2}$ (min)	in vivo hep CL (mL/min/kg)	in vivo hep CL (% LBF)
9a	<0.1	0.4	ND	>60	<39.9	<30
amprenavir[a] /testosterone[b]	0.5[a]	32.7[a]	65.4[a]	6.7[b]	115.2[b]	88[b]
diclofenac[a]/caffeine[b]	47.3[a]	31.2[a]	0.7[a]	>60[b]	<39.9[b]	<30[b]

[a]Reference compounds for the apparent permeability (P_{app}) assay. [b]Reference compounds for metabolic stability assay.

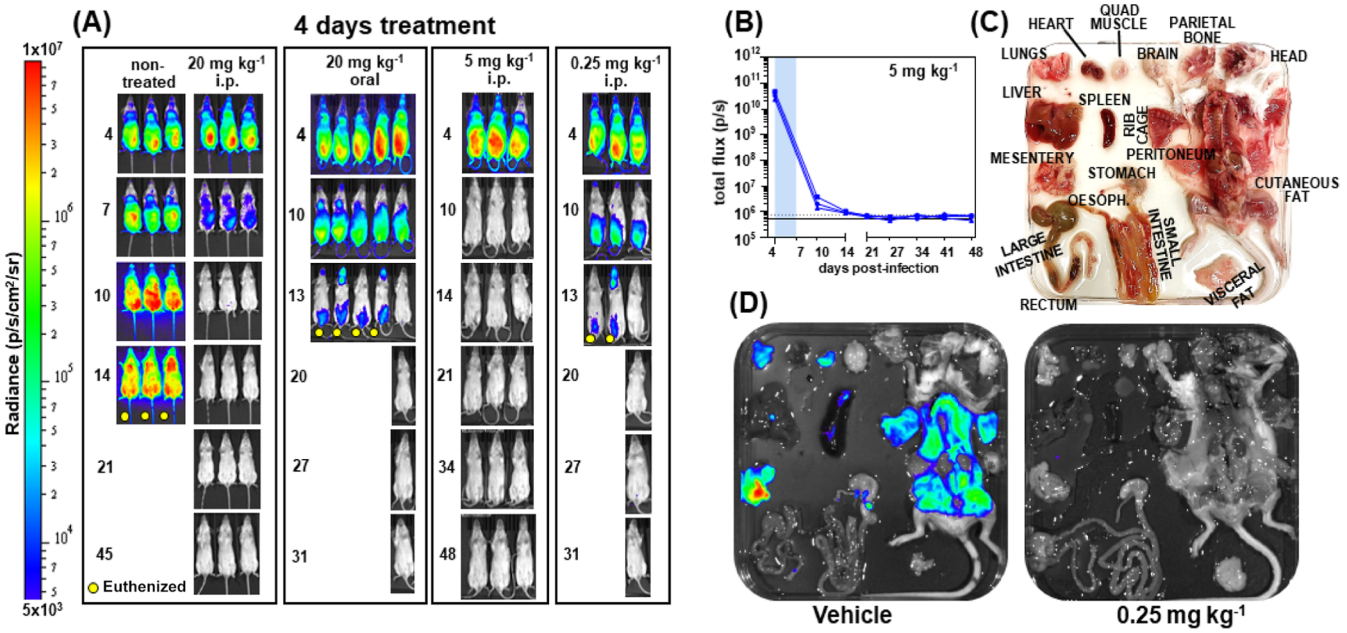

Figure 3. A 4 day treatment regimen with compound **9a** that cures *T. brucei*-infected mice. (A) Ventral images of BALB/c mice infected with bioluminescent *T. brucei* (Experimental Section), following treatment with **9a**. The number of days post-infection is indicated (left). Once daily administration by the i.p. or oral routes was initiated 4 days post-infection at the doses indicated. In accordance with animal welfare requirements, mice designated as non-cured were euthanized (yellow dots). Heat maps are on a log 10 scale and represent the intensity of bioluminescence from low (blue) to high (red). Due to the intense bioluminescent signal exhibited by all mice on day 4 and by non-treated mice at all time points, a less sensitive scale (10^6–10^9 p/s/cm^2/sr) was used in these cases to avoid image saturation. (B) Total body flux for individual mice ($n = 3$) in photons/second (p/s) following treatment at 5 mg kg^{-1}. Data points represent the sum of the total flux from both dorsal and ventral imaging. The treatment period (days 4–7) is indicated by a blue bar. (C) Arrangement of organs and tissues used for ex vivo imaging (Experimental Section). (D) Ex vivo imaging of a non-treated mouse (vehicle, 4 days post-infection) and the 0.25 mg kg^{-1} treated mouse that was negative by in vivo imaging (49 days post-infection). This mouse was designated cured. Bioluminescence intensity is indicated on the scale (left).

2.5. Drug Uptake Studies. The drug pentamidine has been widely used to treat stage 1 African trypanosomiasis.[6] Uptake of this diamidine into *T. brucei* is mediated by an aquaglyceroporin-2 (TbAQP-2) channel protein; parasites where this gene has been deleted are >24-times more resistant than wild types.[49,50] When *Tbaqp* null mutant cell lines were exposed to compound **9a**, sensitivity was slightly reduced (1.3–1.8-fold) (Figure S2A,B), implying that the TbAQPs have a minimal role in facilitating transport of **9a**. To further identify genes that might promote the action of **9a**, we used RNAi target sequencing (RIT-seq) to screen a genome-scale *T. brucei* RNAi library.[49,51] In the library, each parasite contains a random DNA fragment inserted into a single chromosomal locus engineered to facilitate tetracycline-induced expression of double-stranded RNA. Culturing the library in the presence of tetracycline and growth inhibitory levels of a drug of interest has been widely used to identify gene products that drive drug efficacy and whose loss may contribute to resistance (e.g., transporters).[49,52] Despite 3 independent attempts to select resistant parasites, each using a range of compound **9a** concentrations, no outgrowth of resistant parasites was observed (Figure S2C, as an example). This implies that either loss-of-function mechanisms are not relevant to the mode of action or that the major determinant of compound **9a** efficacy is essential for parasite viability and therefore not readily selectable by this approach.

Further assessment of compound **9a** revealed that it is a fluorophore (excitation 550 nm—emission 585 nm). This allowed the uptake and sub-cellular distribution in bloodstream form trypanosomes to be monitored by fluorescence microscopy (Figure 5A). Observations indicated that the compound was initially widely dispersed at a subcellular level but over time became concentrated in an intracellular vesicle characteristic of the lysosome, the acidic vacuole that functions as the terminal location of endocytic cargo.[53,54] To investigate further, we compared the intracellular location of **9a** with LysoTracker, a cell-permeable stain that is highly selective for acidic organelles, including lysosomes. There was considerable overlap (Figure 5B). To provide evidence that **9a** uptake was mediated by endocytosis, we examined the effect of co-

https://doi.org/10.1021/acs.jmedchem.3c01051
J. Med. Chem. XXXX, XXX, XXX−XXX

Table 4. In Vivo Efficacy of Compound 9a against Stage 1 Murine Infections with *T. brucei*[a]

dose	treatment	cure rate
20 mg kg^{-1} i.p.	4 days	3/3
10 mg kg^{-1} i.p.	4 days	3/3
5 mg kg^{-1} i.p.	4 days	3/3
2 mg kg^{-1} i.p.	4 days	4/6
1 mg kg^{-1} i.p.	4 days	3/5
0.5 mg kg^{-1} i.p.	4 days	2/6
0.25 mg kg^{-1} i.p.	4 days	3/6
20 mg kg^{-1} oral	4 days	1/5
20 mg kg^{-1} i.p.	1 day	10/10
10 mg kg^{-1} i.p.	1 day	1/3
5 mg kg^{-1} i.p.	1 day	1/2
2 mg kg^{-1} i.p.	1 day	0/3
1 mg kg^{-1} i.p.	1 day	1/3

[a]Mice were treated by the i.p. or oral routes beginning 4 days post-infection and monitored by bioluminescence imaging (Experimental Section). They were designated as cured if negative by both in vivo and ex vivo imaging (see Figures 3 and 4 as examples).

treatment with sub-lethal levels of bafilomycin A1 (BafA1), an inhibitor of the membrane-localized vacuolar-type proton ATPase (V-type ATPase) that interferes with endosomal trafficking.[55] This multi-subunit complex is responsible for the acidification of intracellular vacuoles, including lysosomes. Co-treatment of trypanosomes conferred a 5−7 fold increase in resistance to **9a** (Figure 6A), a finding that could be correlated with a general reduction in uptake (Figure 6B). To better assess the impact on the endocytic pathway, we co-stained **9a**-treated parasites with an antibody against *T. brucei* cathepsin-L (*Tb*CatL), a cysteine protease specific to the lysosomal/endosomal system.[56] After 6 h exposure, **9a** was predominantly localized to the lysosome and, to a lesser extent, to endosomes. Co-treatment with BafA1 inhibited lysosomal trafficking, with most of the intracellular **9a** restricted to endosomes (Figure 6C). Therefore, treatment of *T. brucei* with an inhibitor of endosomal/lysosomal acidification reduces the uptake and intracellular trafficking of **9a**. We could detect no evidence of localization of the compound to either the nucleus or kinetoplast (Figures 5 and 6).

2.6. Anti-Malarial Activity. Diamidines have been shown to possess anti-malarial activity.[57] We therefore assessed if compound **9a** had activity against *P. falciparum* by investigating its ability to block asexual parasite growth in human blood using a standard in vitro growth inhibition assay (Experimental Section). Over a period of 96 h (2 replication cycles), compound **9a** inhibited asexual development with an EC_{50} of 25.3 nM (Figure 7), indicating cross-species efficacy and representing a 500-fold selectivity over mammalian cells (Table 1).

3. DISCUSSION AND CONCLUSIONS

Recently, we reported on the anti-trypanosomal activity of aromatic benzazole amidines,[34−37] compounds with DNA-

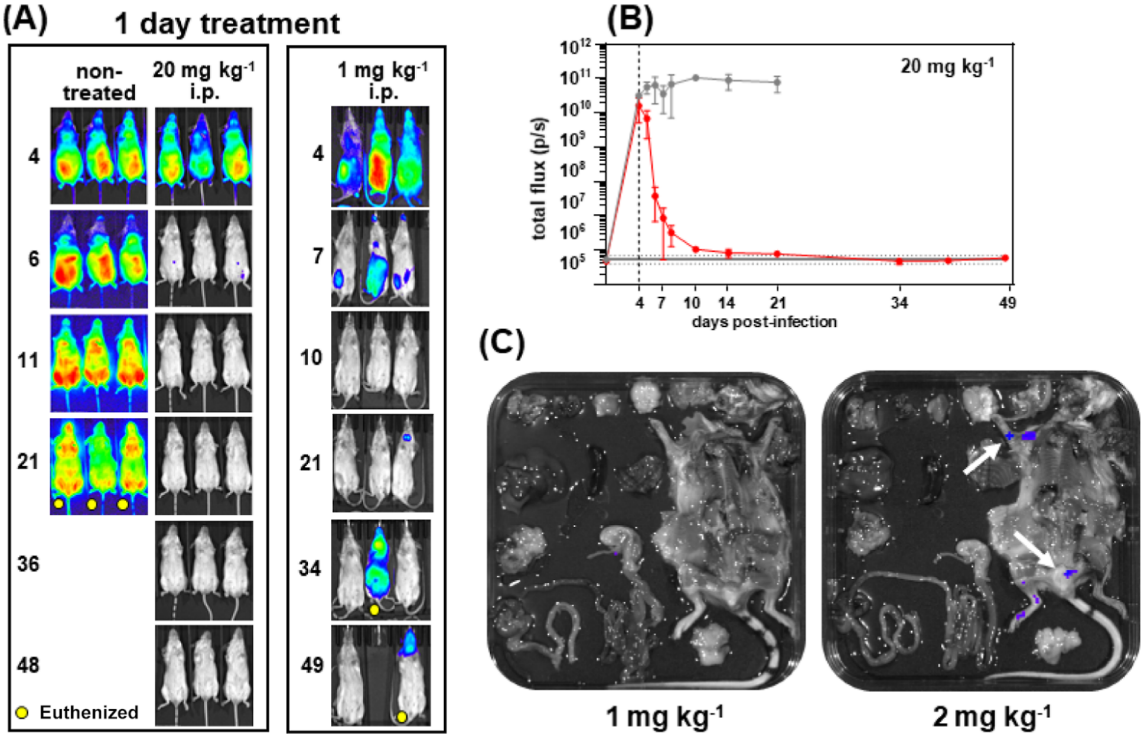

Figure 4. Curing murine *T. brucei* infections with a single dose. (A) Ventral images of *T. brucei*-infected BALB/c mice treated with a single i.p. dose of compound **9a** (Experimental Section). The number of days post-infection is indicated (left). Yellow dots indicate the points at which non-cured mice were euthanized. Heat maps are on a log 10 scale, as shown in Figure 1. The same less sensitive scale, as described in the legend to Figure 1, was used to image the highly bioluminescent non-treated mice. (B) Total body flux of the non-treated mice (grey) and mice treated with a single 20 mg kg^{-1} dose of **9a** (red), 4 days post-infection (n = 3). Data points indicate the mean of the sum of the total flux from both dorsal and ventral imaging. (C) Ex vivo imaging of tissues and organs (arranged as in Figure 3C) from infected mice treated with a single i.p. dose of 1 and 2 mg kg^{-1} **9a**. Images were acquired 49 days post-infection. Mice were designated cured and non-cured, respectively. White arrows indicate faint infection foci in the non-cured mouse. The heat-map scale was the same, as used for Figure 3D.

https://doi.org/10.1021/acs.jmedchem.3c01051
J. Med. Chem. XXXX, XXX, XXX−XXX

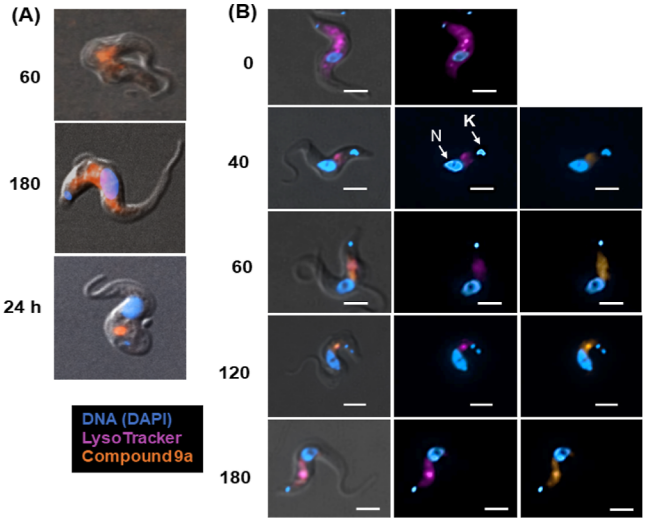

Figure 5. Localization of compound **9a** to the endosomal/lysosomal system in bloodstream form *T brucei*. (A) *T. brucei* were incubated with **9a** (10 μg mL^{-1}) for 60 or 180 min, or for 24 h, and then visualized by fluorescence microscopy (ex. 550 nm; em. 585 nm). (B) LysoTracker (pink) co-localizes with **9a** (orange) in *T. brucei*. Parasites were incubated with **9a** for the time periods indicated (min), stained with LysoTracker, and imaged by fluorescence microscopy (Experimental Section). Merged images, left-hand column. Nuclear (N) and kinetoplast (K) (mitochondrial) DNA are indicated. Note that the parasite shown in the images from 120 min is in the N1K2 stage of the cell cycle, when the mitochondrial, but not nuclear genome, has replicated. Scale bar = 5 μm.

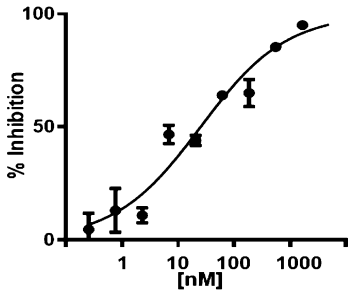

Figure 7. Compound **9a** has activity against asexual forms of the malaria parasite *P. falciparum*. *P. falciparum* 3D7 strain asexual parasites were cultured in human erythrocytes with compound **9a** for 96 h (Experimental Section). Dose response curves were established from three independent experiments, and the EC_{50} value was calculated (25.3 nM).

binding properties. Here, we have extended this work by synthesizing a series of head-to-head bis-6-amidino-benzothiazoles containing alkyl, cycloalkyl, or alkenyl spacers. This has led to the identification of *trans*-2,2′-(cyclohexane-1,4-diyl)bis-6-amidiniumbenzothiazole dimethansulfonate (**9a**), a compound with sub-nanomolar trypanocidal activity (Scheme 1, Table 1). In this molecule, the central cyclohexyl component and the unsubstituted amidino moieties are the crucial determinants of efficacy. The compound displayed impressive in vivo activity. After 4 days of i.p. treatment at 5 mg kg^{-1}, parasites were undetectable in all cases, with no relapse. Curative potential was observed at doses down to 0.25 mg kg^{-1} (Figure 3). Oral administration was less effective, probably reflecting the low permeability of the compound (Table 3). However, the extent of parasite knockdown achieved with oral dosing, which in one case led to complete clearance (Figure 3A), suggests that minor modifications to the molecule could be sufficient to enhance bioavailability and lead to more consistent curative outcomes. Of particular note were the results achieved with single dosing, which resulted in parasite clearance in all cases at 20 mg kg^{-1} (10/10) (Figure 4, Table 4). Translation of such an outcome to a clinical setting would represent a significant advance since pentamidine, the current front-line treatment for juvenile stage 1 infections, requires 7 daily intramuscular injections under medical supervision.[58]

Diamidines such as pentamidine and the veterinary drug diminazene aceturate (berenil) bind to the minor groove of parasite DNA, a property that has been implicated in their mode of action.[59] Monitoring uptake of fluorescent diamidines has shown that these drugs accumulate rapidly in the parasite mitochondrion (the kinetoplast)[60] and bind to mitochondrial

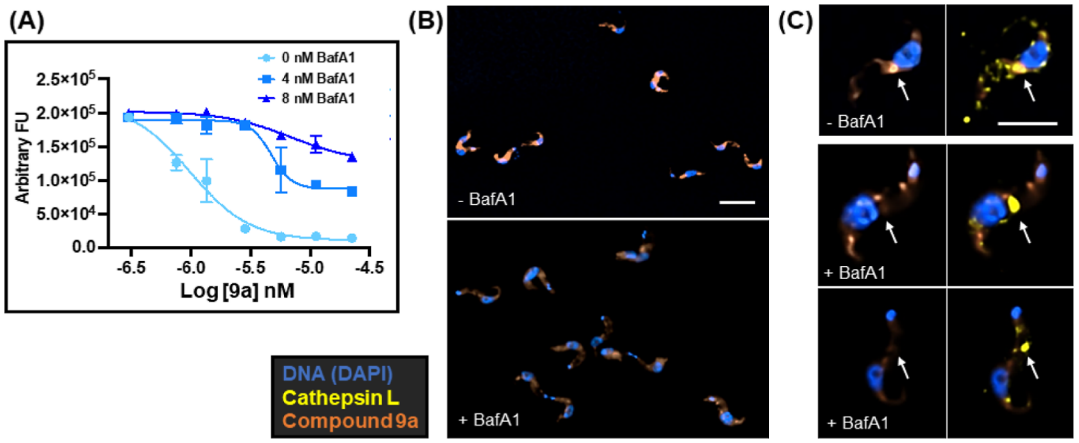

Figure 6. Inhibitor of endosomal/lysosomal acidification reduces compound **9a** uptake and trafficking in bloodstream form *T. brucei*. (A) Impact of **9a** on trypanosome growth at different concentrations of bafilomycin A1 (BafA1), as indicated. Experiments were performed in triplicate, with parasite growth inferred from resazurin reduction assays (Experimental Section). (B) Fluorescence images of trypanosomes incubated with **9a** (10 μg mL^{-1}) for 6 h in the presence or absence of BafA1 (8 nM). Scale bar = 20 μm. (C) Fluorescence images of trypanosomes incubated with **9a** in the presence of BafA1 (as above) and stained with an antibody against TbCatL (Experimental Section). White arrows indicate the location of the single lysosomal vesicle (bright yellow), with the smaller yellow dots indicating the location of endosomal vacuoles. Note the absence of **9a** lysosomal fluorescence (orange) in the BafA1-treated parasites.

https://doi.org/10.1021/acs.jmedchem.3c01051
J. Med. Chem. XXXX, XXX, XXX−XXX

DNA (kDNA). However, their use against stage 2 trypanosomiasis is limited by their inability to cross the BBB at levels sufficient to eliminate CNS infections. Here, we found that a 3 day treatment regimen with **9a** was also unable to cure stage 2 infections, although it could provide a substantial (>99.99%) and prolonged knockdown of the parasite burden (Figure S1). Parasite survival/relapse was largely restricted to the cranial region. Therefore, the compound will require further re-engineering to enhance CNS penetration. Transmembrane diffusion is the most common route by which drugs cross the BBB,[61] and the low permeability of **9a** (Table 3) could be a critical factor that blocks or reduces access into the CNS.

The low permeability of **9a** also implied that diffusion through the parasite cell membrane was unlikely to be a significant uptake mechanism. Accordingly, we found evidence that entry into *T. brucei* was mediated by endocytosis (Figures 5 and 6). Among eukaryotes, trypanosomes have one of the fastest rates of endocytosis, with the process occurring exclusively via the flagellar pocket.[62,63] Fluorescence imaging revealed sequestration of **9a** within the lysosome or other acidic vacuoles (Figure 5). We also found that uptake and trafficking to the lysosome could be inhibited by BafA1 (Figure 6). This macrolide antibiotic inhibits V-type ATPase-mediated endosomal acidification,[55] affecting both fluid phase and receptor-mediated endocytosis and blocking the maturation pathway of early to late endosomes.[64,65] Although BafA1 is also a potassium ionophore and inhibits mitochondrial function,[66,67] this only occurs at levels 20 times higher than the BafA1 concentrations used in the current study (Figure 6). Unlike pentamidine, aquaglyceroporins do not have a significant role in **9a** uptake (Figure S2), and a genome-wide screen using RIT-seq[49,51] failed to identify alternative transporters that might be involved. Importantly, this reduces the likelihood of pentamidine:**9a** cross-resistance. To further explore resistance mechanisms, we attempted to select **9a**-resistant parasites for genome analysis. However, all attempts, under a range of conditions, were unsuccessful.

The possibility that **9a** trypanocidal activity might involve disruption of some aspect of endosomal/lysosomal function remains to be established and will be an important focus of future research. The absence of co-localization with either the nucleus or kinetoplast (the mitochondrial genome) (Figures 5 and 6) suggests that DNA binding activity does not have a role in the mode of action, as has been proposed for other diamidine drugs.[59,68] However, it is clear that **9a** has a slow-acting cytotoxic mode of action and that 3 days exposure to concentrations of 1.2 nM and above results in inevitable parasite cell death, even if the compound is removed. In the case of *P. falciparum*, dissecting the mechanism of uptake is more complex because drugs must cross the erythrocyte plasma membrane, the parasitophorous vacuole membrane, and the parasite plasma membrane. Intriguingly, pentamidine is selectively concentrated 500-fold within erythrocytes that are *Plasmodium*-infected but not within those that are non-infected, implying that the mechanism of uptake is a specific process.[57] This is thought to involve the new permeation pathways that are generated within infected erythrocytes, which are required for parasite acquisition of essential nutrients and vitamins from host serum.[69] These pathways may provide a route for the uptake of **9a** into infected erythrocytes.

In summary, we have identified a novel bis-6-amidinobenzothiazole that can eliminate stage 1 *T. brucei* infections in experimental murine models. This lead compound has clinical and veterinary potential, with the possibility of enhanced applications following further structural modification.

4. EXPERIMENTAL SECTION

4.1. Chemistry. *4.1.1. General Information.* Melting points were determined using an Original Kofler Mikroheitztisch apparatus (Reichert, Wien). ^{1}H NMR and ^{13}C NMR spectra were recorded with the Bruker Avance DPX-300 or Bruker AV-600 using tetramethylsilane as the internal standard. Chemical shifts are reported in parts per million (ppm) relative to TMS. UPLC-MS spectra were recorded with Agilent 1290 Infiniti II/6120 Quadrupole LC/MS spectrometers using electrospray ionization (ESI). HPLC spectra were recorded with the Agilent 1100 LC System. All prepared compounds had a purity of ≥95%, determined by HPLC. Elemental analyses for carbon, hydrogen, and nitrogen were performed on the PerkinElmer 2400 elemental analyzer. Analyses are indicated as symbols of elements, and the analytical results obtained are within ±0.4% of the theoretical value. The synthesis of 2-amino-5-amidiniumbenzenethiolate (**1a**), 2-amino-5-(4,5-dihydro-1*H*-imidazol-3-ium-2-yl)benzenethiolate hydrate (**1b**), and 2-amino-5-(3,4,5,6-tetrahydropyrimidin-1-ium-2 yl)benzenethiolate (**1c**) was carried out as described.[42,43]

*4.1.2. General Procedure for the Preparation of Compounds **3a−10c**.* A mixture of 5-amidino-substituted 2-aminothiophenol **1a−1c** (1.0 equiv) and a corresponding dicarboxylic acid **2a−2h** (0.5 equiv) in polyphosphoric acid (PPA) was heated at 120−130 °C until the mixture became homogenous and then at 180 °C for 2 h. The reaction mixture was poured into water (100−150 mL), cooled, and made alkaline with 20% NaOH. The resulting free base was filtered, washed with water, and dried under vacuum over KOH. The crude free base was converted into a methanesulfonate salt, as described below.

*4.1.2.1. 2,2′-(Ethane-1,2-diyl)bis-6-amidiniumbenzothiazole Dimethansulfonate (**3a**).* 2-Amino-5-amidiniumbenzenethiolate (**1a**) (168 mg, 1.0 mmol) and succinic acid (**2a**) (60 mg, 0.5 mmol) were heated in PPA (9.6 g). The resulting crude free base was then suspended in EtOH (20 mL), and methanesulfonic acid (130 μL, 2.0 mmol) was added and stirred at room temperature for 2 h. After cooling overnight, the resulting precipitate was filtered, crystallized from the water/acetone mixture, and dried at 75 °C. The yield of pure compound **3a** as a white solid was 174 mg (58%); mp > 300 °C. UPLC (230 nm): 100 area %; MS (ESI): m/z = 191.2 (M + 2H$^+$)/2 calcd for free base 380.09. ^{1}H NMR (300 MHz, DMSO-d_6) (δ ppm): 9.35 (br s, 4H, −C(NH_2)$_2^+$), 9.11 (br s, 4H, −C(NH_2)$_2^+$), 8.57 (d, 2H, J = 1.6 Hz, Ar−H), 8.15 (d, 2H, J = 8.5 Hz, Ar−H), 7.86 (dd, 2H, J = 8.5 Hz, J = 1.6 Hz, Ar−H), 3.84 (s, 4H, −CH_2CH_2−), 2.36 (s, 6H, CH_3SO$_3^-$). ^{13}C NMR (75 MHz, D_2O) (δ ppm): 176.1 (s), 166.2 (s), 155.1 (s), 135.2 (s), 125.6 (d), 124.6 (s), 122.5 (d), 122.3 (d), 38.4 (q), 32.5 (t). Analysis calculated for $C_{20}H_{24}N_6O_6S_4$·1.5H_2O (599.73): C, 40.05; H, 4.54; N, 14.01. Found: C, 40.12; H, 4.61; N, 13.90.

*4.1.2.2. 2,2′-(Ethane-1,2-diyl)bis-6-(4,5-dihydro-1H-imidazolium-2-yl)benzothiazole Dimethansulfonate (**3b**).* 2-Amino-5-(4,5-dihydro-1*H*-imidazol-3-ium-2-yl)benzenethiolate hydrate (**1b**) (106 mg, 0.50 mmol) and succinic acid (**2a**) (30 mg, 0.25 mmol) were heated in PPA (8.3 g), and the crude free base was suspended in 2-PrOH (10 mL), and methanesulfonic acid (65 μL, 1.0 mmol) was added and stirred at room temperature for 3 h. After cooling overnight, the resulting precipitate was filtered and dried at 75 °C. The yield of pure compound **3b** as a white solid was 120 mg (71%); mp > 300 °C. UPLC (230 nm): 99.4 area %; MS (ESI): m/z = 217.2 (M + 2H$^+$)/2 calcd for free base 432.12. ^{1}H NMR (300 MHz, DMSO-d_6) (δ ppm): 10.55 (s, 4H, −C(NH−)$_2^+$), 8.68 (s, 2H, Ar−H), 8.21 (d, 2H, J = 8.5 Hz, Ar−H), 7.98 (d, 2H, J = 8.5 Hz, Ar−H), 4.07 (s, 2H, −CH_2CH_2−), 4.04 (s, 8H, −CH_2CH_2−), 3.86 (s, 4H, −CH_2CH_2−), 2.31 (s, 6H, CH_3SO$_3^-$). ^{13}C NMR (75 MHz, D_2O) (δ ppm): 176.5 (s), 165.6 (s), 155.3 (s), 135.4 (s), 125.7 (d), 122.8 (d), 122.4 (d), 118.7 (s), 44.6 (t), 38.4 (q), 32.2 (t). Analysis calculated for

https://doi.org/10.1021/acs.jmedchem.3c01051
J. Med. Chem. XXXX, XXX, XXX−XXX

$C_{24}H_{28}N_6O_6S_4 \cdot 3H_2O$ (678.82): C, 42.46; H, 5.05; N, 12.38. Found: C, 42.54; H, 4.92; N, 12.39.

*4.1.2.3. 2,2′-(Ethane-1,2-diyl)bis-6-(3,4,5,6-tetrahydropyrimidinium-2-yl)benzothiazole Dimethansulfonate (**3c**).* 2-Amino-5-(3,4,5,6-tetrahydropyrimidin-1-ium-2-yl)benzenethiolate (**1c**) (0.105 g, 0.5 mmol) and succinic acid (**2a**) (30 mg, 0.25 mmol) were heated in PPA (10.2 g). The obtained crude free base was dissolved in EtOH (5 mL), and methanesulfonic acid (65 μL, 1.0 mmol) was added, stirred at room temperature for 1 h, and precipitated by the addition of diethyl ether. The resulting precipitate was filtered, crystallized from the water/acetone mixture, and dried at 75 °C. The yield of pure compound **3c** as a white hygroscopic solid was 69 mg (39%); mp = 292−297 °C (dec.). HPLC (220 nm): 98.1 area %; MS (ESI): m/z = 231.4 (M + 2H$^+$)/2 calcd for free base 462.16. ^{1}H NMR (300 MHz, DMSO-d_6) (δ ppm): 10.00 (s, 4H, −C(N*H*−)$_2^+$), 8.48 (d, 2H, J = 1.6 Hz, Ar−*H*), 8.15 (d, 2H, J = 8.6 Hz, Ar−*H*), 7.78 (dd, 2H, J = 8.6 Hz, J = 1.6 Hz, Ar−*H*), 3.83 (s, 4H, −C*H*$_2$C*H*$_2$−), 3.51 (t, 8H, J = 5.0 Hz, −C(NH$^+$C*H*$_2$)$_2$−), 2.36 (s, 6H, C*H*$_3$SO$_3^-$), 2.00 (m, 4H, J = 5.0 Hz, −C(NH$^+$CH$_2$)$_2$C*H*$_2$−). ^{13}C NMR (75 MHz, DMSO-d_6) (δ ppm): 174.2 (s), 159.2 (s), 155.2 (s), 135.1 (s), 125.5 (d), 125.1 (s), 122.6 (d), 39.7 (q), 38.9 (t), 32.4 (t), 17.7 (t). Analysis calculated for $C_{26}H_{32}N_6O_6S_4 \cdot 3H_2O$ (706.87): C, 44.18; H, 5.42; N, 11.89. Found: C, 44.42; H, 5.08; N, 12.05.

*4.1.2.4. 2,2′-(Propane-1,3-diyl)bis-6-amidiniumbenzothiazole Dimethansulfonate (**4a**).* 2-Amino-5-amidiniumbenzenethiolate (**1a**) (134 mg, 0.8 mmol) and glutaric acid (**2b**) (53 mg, 0.4 mmol) were heated in PPA (9.5 g). The resulting crude free base was suspended in EtOH (10 mL), and methanesulfonic acid (105 μL, 1.6 mmol) was added and stirred at room temperature for 2 h. After cooling overnight, the resulting precipitate was filtered, crystallized from the water/acetone mixture, and dried at 75 °C. The yield of pure compound **4a** as a white solid was 104 mg (43%); mp = 237−241 °C. HPLC (220 nm): 98.6 area %; MS (ESI): m/z = 198.4 (M + 2H$^+$)/2 calcd for free base 394.10. ^{1}H NMR (300 MHz, DMSO-d_6) (δ ppm): 9.39 (s, 4H, −C(N*H*$_2$)$_2^+$), 9.09 (s, 4H, −C(N*H*$_2$)$_2^+$), 8.60 (d, 2H, J = 1.6 Hz, Ar−*H*), 8.16 (d, 2H, J = 8.6 Hz, Ar−*H*), 7.88 (dd, 2H, J = 8.6 Hz, J = 1.6 Hz, Ar−*H*), 2.36 (s, 6H, C*H*$_3$SO$_3^-$). ^{1}H NMR (300 MHz, D$_2$O) (δ ppm): 8.17 (d, 2H, J = 1.6 Hz, Ar−*H*), 7.72 (d, 2H, J = 8.5 Hz, Ar−*H*), 7.62 (dd, 2H, J = 8.5 Hz, J = 1.6 Hz, Ar−*H*), 3.20 (t, 4H, J = 6.9 Hz, −C*H*$_2$CH$_2$C*H*$_2$−), 2.79 (s, 6H, C*H*$_3$SO$_3^-$), 2.36 (m, 2H, J = 6.9 Hz, −CH$_2$C*H*$_2$CH$_2$−). ^{13}C NMR (75 MHz, D$_2$O) (δ ppm): 178.2 (s), 165.8 (s), 155.0 (s), 135.1 (s), 125.2 (d), 123.9 (s), 122.1 (d), 121.6 (d), 38.4 (q), 32.7 (t), 28.1 (t). Analysis calculated for $C_{21}H_{26}N_6O_6S_4 \cdot H_2O$ (604.74): C, 41.71; H, 4.67; N, 13.90. Found: C, 41.88; H, 4.63; N, 11.78.

*4.1.2.5. 2,2′-(Propane-1,3-diyl)bis-6-(4,5-dihydro-1H-imidazolium-2-yl)benzothiazole Dimethansulfonate (**4b**).* 2-Amino-5-(4,5-dihydro-1*H*-imidazol-3-ium-2-yl)benzenethiolate hydrate (**1b**) (106 mg, 0.50 mmol) and glutaric acid (**2b**) (33 mg, 0.25 mmol) were heated in PPA (10.1 g). The crude free base then was dissolved in 2-PrOH (15 mL), and methanesulfonic acid (65 μL, 1.0 mmol) was added and stirred at room temperature for 2 h. After cooling overnight, the resulting precipitate was filtered, crystallized from the water/acetone mixture, and dried at 75 °C. The yield of pure compound **4b** as a white solid was 86 mg (52%); mp = 235−239 °C. UPLC (254 nm): 100 area %; MS (ESI): m/z = 224.2 (M + 2H$^+$)/2 calcd for free base 446.13. ^{1}H NMR (300 MHz, DMSO-d_6) (δ ppm): 10.57 (s, 4H, −C(N*H*−)$_2^+$), 8.71 (d, 2H, J = 1.4 Hz, Ar−*H*), 8.22 (d, 2H, J = 8.6 Hz, Ar−*H*), 8.00 (dd, 2H, J = 8.6 Hz, J = 1.4 Hz, Ar−*H*), 4.05 (s, 8H, −C*H*$_2$C*H*$_2$−), 2.33 (s, 6H, C*H*$_3$SO$_3^-$). ^{1}H NMR (300 MHz, D$_2$O) (δ ppm): 8.13 (s, 2H, Ar−*H*), 7.65 (d, 2H, J = 8.5 Hz, Ar−*H*), 7.56 (d, 2H, J = 8.5 Hz, Ar−*H*), 4.08 (s, 2H, −C*H*$_2$C*H*$_2$−), 3.20 (t, 4H, J = 6.6 Hz, −C*H*$_2$CH$_2$C*H*$_2$−), 2.79 (s, 6H, C*H*$_3$SO$_3^-$), 2.36 (m, 2H, J = 6.6 Hz, −CH$_2$C*H*$_2$CH$_2$−). ^{13}C NMR (75 MHz, D$_2$O) (δ ppm): 178.6 (s), 165.4 (s), 155.1 (s), 135.3 (s), 125.2 (d), 122.5 (d), 121.9 (d), 118.0 (s), 44.6 (t), 38.4 (q), 32.8 (t), 28.0 (t). Analysis calculated for $C_{25}H_{30}N_6O_6S_4 \cdot 1.25H_2O$ (661.32): C, 45.40; H, 4.95; N, 12.71. Found: C, 45.35; H, 5.22; N, 12.64.

*4.1.2.6. 2,2′-(Butane-1,4-diyl)bis-6-amidiniumbenzothiazole Dimethansulfonate (**5a**).* 2-Amino-5-amidiniumbenzenethiolate (**1a**) (84 mg, 0.5 mmol) and adipic acid (**2c**) (36 mg, 0.25 mmol) were heated in PPA (8.2 g). The resulting crude free base was suspended in EtOH (10 mL), and methanesulfonic acid (65 μL, 1.0 mmol) was added and stirred at room temperature for 1 h. After cooling overnight, the resulting precipitate was filtered, crystallized from the water/acetone mixture, and dried at 75 °C. The yield of pure compound **5a** as a white solid was 91 mg (57%); mp > 300 °C. UPLC (230 nm): 100 area %; MS (ESI): m/z = 205.2 (M + 2H$^+$)/2 calcd for free base 408.12. ^{1}H NMR (300 MHz, DMSO-d_6) (δ ppm): 9.38 (br s, 4H, −C(N*H*$_2$)$_2^+$), 9.06 (br s, 4H, −C(N*H*$_2$)$_2^+$), 8.58 (d, 2H, J = 1.5 Hz, Ar−*H*), 8.14 (d, 2H, J = 8.6 Hz, Ar−*H*), 7.86 (dd, 2H, J = 8.6 Hz, J = 1.6 Hz, Ar−*H*), 2.35 (s, 6H, C*H*$_3$SO$_3^-$), 1.99 (br s, 4H, −CH$_2$(C*H*$_2$)$_2$CH$_2$−). ^{1}H NMR (300 MHz, D$_2$O) (δ ppm): 8.22 (s, Ar−*H*), 7.85 (d, 2H, J = 8.5 Hz, Ar−*H*), 7.73 (d, 2H, J = 8.5 Hz, Ar−*H*), 3.08 (br s, 4H, −C*H*$_2$(CH$_2$)$_2$C*H*$_2$−), 2.79 (s, 6H, C*H*$_3$SO$_3^-$), 1.84 (br s, 4H, −CH$_2$(C*H*$_2$)$_2$CH$_2$−). ^{13}C NMR (75 MHz, D$_2$O) (δ ppm): 180.0 (s), 166.0 (s), 155.2 (s), 135.1 (s), 125.4 (d), 124.1 (s), 122.3 (d), 122.0 (d), 38.4 (q), 32.9 (t), 27.8 (t). Analysis calculated for $C_{22}H_{28}N_6O_6S_4 \cdot 2H_2O$ (636.78): C, 41.50; H, 5.07; N, 13.20. Found: C, 41.36; H, 5.04; N, 13.33.

*4.1.2.7. 2,2′-(Butane-1,4-diyl)bis-6-(4,5-dihydro-1H-imidazolium-2-yl)benzothiazole Dimethansulfonate (**5b**).* 2-Amino-5-(4,5-dihydro-1*H*-imidazol-3-ium-2-yl)benzenethiolate hydrate (**1b**) (106 mg, 0.50 mmol) and adipic acid (**2c**) (36 mg, 0.25 mmol) were heated in PPA (10.2 g). The crude free base was then suspended in 2-PrOH (10 mL), and methanesulfonic acid (65 μL, 1.0 mmol) was added and stirred at room temperature for 1 h. After cooling overnight, the resulting precipitate was filtered, crystallized from the water/acetone mixture, and dried at 75 °C. The yield of pure compound **5b** as a white solid was 110 mg (63%); mp = 270−275 °C (dec.). UPLC (254 nm): 96.8 area %; MS (ESI): m/z = 461.2 (M + H$^+$) calcd for free base 460.15. ^{1}H NMR (300 MHz, DMSO-d_6) (δ ppm): 10.56 (s, 4H, −C(N*H*−)$_2^+$), 8.69 (d, 2H, J = 1.6 Hz, Ar−*H*), 8.20 (d, 2H, J = 8.6 Hz, Ar−*H*), 7.98 (dd, 2H, J = 8.6 Hz, J = 1.6 Hz, Ar−*H*), 4.05 (s, 8H, −C*H*$_2$C*H*$_2$−), 3.29 (br s, 4H, −C*H*$_2$(CH$_2$)$_2$C*H*$_2$−), 2.31 (s, 6H, C*H*$_3$SO$_3^-$), 2.00 (br s, 4H, −CH$_2$(C*H*$_2$)$_2$CH$_2$−). ^{13}C NMR (75 MHz, D$_2$O) (δ ppm): 179.4 (s), 165.6 (s), 155.4 (s), 135.2 (s), 125.5 (d), 122.7 (d), 122.1 (d), 118.2 (s), 44.6 (t), 38.4 (q), 32.9 (t), 27.8 (t). Analysis calculated for $C_{26}H_{32}N_6O_6S_4 \cdot 2.5H_2O$ (697.86): C, 44.75; H, 5.34; N, 12.04. Found: C, 44.81; H, 5.38; N, 11.99.

*4.1.2.8. 2,2′-(Butane-1,4-diyl)bis-6-(3,4,5,6-tetrahydropyrimidinium-2-yl)benzothiazole Dimethansulfonate (**5c**).* 2-Amino-5-(3,4,5,6-tetrahydropyrimidin-1-ium-2-yl)benzenethiolate (**1c**) (0.105 g, 0.5 mmol) and adipic acid (**2c**) (36 mg, 0.25 mmol) were heated in PPA (9.2 g). The resulting crude free base was then dissolved in EtOH (5 mL), and methanesulfonic acid (65 μL, 1.0 mmol) was added, stirred at room temperature for 1 h, and precipitated by the addition of diethyl ether. The resulting precipitate was filtered and dried at 75 °C. The yield of pure compound **5c** as a white hygroscopic solid was 88 mg (47%); mp = 169−176 °C. UPLC (230 nm): 99.5 area %; MS (ESI): m/z = 245.4 (M + 2H$^+$)/2 calcd for free base 488.18. ^{1}H NMR (600 MHz, DMSO-d_6) (δ ppm): 9.99 (s, 4H, −C(N*H*−)$_2^+$), 8.48 (d, 2H, J = 1.7 Hz, Ar−*H*), 8.15 (d, 2H, J = 8.6 Hz, Ar−*H*), 7.78 (dd, 2H, J = 8.6 Hz, J = 1.7 Hz, Ar−*H*), 3.52 (br s, 8H, −C(NH$^+$CH$_2$)$_2$−), 3.28 (t, 4H, J = 5.9 Hz, −CH$_2$(CH$_2$)$_2$CH$_2$−), 2.31 (s, 6H, C*H*$_3$SO$_3^-$), 2.03−1.96 (m, 8H, −CH$_2$(C*H*$_2$)$_2$C*H*$_2$− + −C(NH$^+$CH$_2$)$_2$C*H*$_2$). ^{13}C NMR (150 MHz, DMSO-d_6) (δ ppm): 176.0 (s), 159.2 (s), 155.5 (s), 135.0 (s), 125.3 (d), 124.9 (s), 122.4 (d), 39.7 (q), 38.9 (t), 33.2 (t), 28.0 (t), 17.7 (t). Analysis calculated for $C_{28}H_{36}N_6O_6S_4 \cdot 4H_2O$ (752.94): C, 44.66; H, 5.89; N, 11.16. Found: C, 44.45; H, 5.99; N, 11.18.

*4.1.2.9. 2,2′-(Pentane-1,5-diyl)bis-6-amidiniumbenzothiazole Dimethansulfonate (**6a**).* 2-Amino-5-amidiniumbenzenethiolate (**1a**) (84 mg, 0.5 mmol) and pimelic acid (**2d**) (40 mg, 0.25 mmol) were heated in PPA (10.3 g). The resulting crude free base was then suspended in 2-PrOH (10 mL), and methanesulfonic acid (65 μL, 1.0 mmol) was added and stirred at room temperature for 1 h. After cooling overnight, the resulting precipitate was filtered, crystallized from the water/acetone mixture, and dried at 75 °C.

https://doi.org/10.1021/acs.jmedchem.3c01051
J. Med. Chem. XXXX, XXX, XXX−XXX

The yield of pure compound **6a** as a white solid was 82 mg (50%); mp = 258−262 °C (dec.). UPLC (254 nm): 99.2 area %; MS (ESI): m/z = 212.3 (M + 2H$^+$)/2 calcd for free base 422.13. ^{1}H NMR (300 MHz, DMSO-d_6) (δ ppm): 9.22 (br s, 8H, −C(NH_2)$_2^+$), 8.57 (d, 2H, J = 1.7 Hz, Ar−H), 8.13 (d, 2H, J = 8.6 Hz, Ar−H), 7.86 (dd, 2H, J = 8.6 Hz, J = 1.7 Hz, Ar−H), 3.21 (t, 4H, J = 7.4 Hz, −CH_2(CH$_2$)$_3$CH_2−), 2.35 (s, 6H, CH_3SO$_3^-$), 1.92 (m, 4H, J = 7.4 Hz, −CH$_2$CH_2CH$_2$CH_2CH$_2$−), 1.57−1.48 (m, 2H, −(CH$_2$)$_2$CH_2(CH$_2$)$_2$−). ^{13}C NMR (75 MHz, D$_2$O) (δ ppm): 179.5 (s), 165.8 (s), 155.1 (s), 135.0 (s), 125.2 (d), 123.7 (s), 122.1 (d), 121.8 (d), 38.4 (q), 32.8 (t), 27.7 (t), 26.6 (t). Analysis calculated for C$_{23}$H$_{30}$N$_6$O$_6$S$_4$·2.5H$_2$O (659.82): C, 41.87; H, 5.35; N, 12.74. Found: C, 42.05; H, 5.56; N, 12.65.

*4.1.2.10. 2,2′-(Pentane-1,5-diyl)bis-6-(4,5-dihydro-1H-imidazolium-2-yl)benzothiazole Dimethansulfonate (**6b**).* 2-Amino-5-(4,5-dihydro-1H-imidazol-3-ium-2-yl)benzenethiolate hydrate (**1b**) (106 mg, 0.50 mmol) and pimelic acid (**2d**) (40 mg, 0.25 mmol) were heated in PPA (10.8 g). The crude free base was then suspended in 2-PrOH (10 mL), and methanesulfonic acid (65 μL, 1.0 mmol) was added and stirred at room temperature for 2 h. After cooling overnight, the resulting precipitate was filtered, crystallized from the water/acetone mixture, and dried at 75 °C. The yield of pure compound **6b** as a beige solid was 87 mg (48%); mp = 192−197 °C. UPLC (254 nm): 100 area %; MS (ESI): m/z = 238.3 (M + 2H$^+$)/2 calcd for free base 474.17. ^{1}H NMR (300 MHz, DMSO-d_6) (δ ppm): 10.55 (br s, 4H, −C(NH−)$_2^+$), 8.68 (d, 2H, J = 1.7 Hz, Ar−H), 8.19 (d, 2H, J = 8.6 Hz, Ar−H), 7.98 (dd, 2H, J = 8.6 Hz, J = 1.7 Hz, Ar−H), 4.05 (s, 8H, −CH_2CH_2−), 3.22 (t, 4H, J = 7.5 Hz, −CH_2(CH$_2$)$_3$CH_2−), 2.32 (s, 6H, CH_3SO$_3^-$), 1.92 (m, 4H, J = 7.5 Hz, −CH$_2$CH_2CH$_2$CH_2CH$_2$−), 1.59−1.49 (m, 2H, −(CH$_2$)$_2$CH_2(CH$_2$)$_2$−). ^{13}C NMR (75 MHz, D$_2$O) (δ ppm): 180.1 (s), 165.5 (s), 155.4 (s), 135.3 (s), 125.4 (d), 122.7 (d), 122.1 (d), 118.1 (s), 44.8 (t), 38.6 (q), 33.1 (t), 27.9 (t), 27.2 (t). Analysis calculated for C$_{27}$H$_{34}$N$_6$O$_6$S$_4$·3H$_2$O (720.90): C, 44.98; H, 5.59; N, 11.66. Found: C, 45.12; H, 5.59; N, 11.65.

*4.1.2.11. 2,2′-(Hexane-1,6-diyl)bis-6-amidiniumbenzothiazole Dimethansulfonate (**7a**).* 2-Amino-5-amidiniumbenzenethiolate (**1a**) (84 mg, 0.5 mmol) and suberic acid (**2e**) (44 mg, 0.25 mmol) were heated in PPA (10.0 g). The resulting crude free base was suspended in 2-PrOH (10 mL), and methanesulfonic acid (65 μL, 1.0 mmol) was added and stirred at room temperature for 4 h. After cooling overnight, the resulting precipitate was filtered, crystallized from the water/acetone mixture, and dried at 75 °C. The yield of pure compound **7a** as a white solid was 71 mg (43%); mp = 295−300 °C (dec.). UPLC (254 nm): 96.0 area %; MS (ESI): m/z = 219.2 (M + 2H$^+$)/2 calcd for free base 436.15. ^{1}H NMR (300 MHz, DMSO-d_6) (δ ppm): 9.21 (br s, 8H, −C(NH_2)$_2^+$), 8.57 (d, 2H, J = 1.6 Hz, Ar−H), 8.14 (d, 2H, J = 8.6 Hz, Ar−H), 7.86 (dd, 2H, J = 8.6 Hz, J = 1.6 Hz, Ar−H), 3.19 (t, 4H, J = 7.5 Hz, −CH_2(CH$_2$)$_4$CH_2−), 2.35 (s, 6H, CH_3SO$_3^-$), 1.85 (m, 4H, J = 7.4 Hz, −CH$_2$CH_2(CH$_2$)$_2$CH_2CH$_2$−), 1.47 (br s, 4H, −(CH$_2$)$_2$(CH_2)$_2$(CH$_2$)$_2$−). ^{13}C NMR (75 MHz, D$_2$O) (δ ppm): 179.8 (s), 166.01 (s), 155.2 (s), 135.1 (s), 125.4 (d), 124.0 (s), 122.3 (d), 121.9 (d), 38.4 (q), 33.2 (t), 28.3 (t), 27.6 (t). Analysis calculated for C$_{24}$H$_{32}$N$_6$O$_6$S$_4$·2H$_2$O (664.84): C, 43.36; H, 5.46; N, 12.64. Found: C, 43.45; H, 5.33; N, 12.65.

*4.1.2.12. 2,2′-(Hexane-1,6-diyl)bis-6-(4,5-dihydro-1H-imidazolium-2-yl)benzothiazole Dimethansulfonate (**7b**).* 2-Amino-5-(4,5-dihydro-1H-imidazol-3-ium-2-yl)benzenethiolate hydrate (**1b**) (106 mg, 0.50 mmol) and suberic acid (**2e**) (44 mg, 0.25 mmol) were heated in PPA (10.6 g). Afterward, the crude free base was suspended in 2-PrOH (10 mL), and methanesulfonic acid (65 μL, 1.0 mmol) was added and stirred at room temperature for 1 h. After cooling overnight, the resulting precipitate was filtered, crystallized from the water/acetone mixture, and dried at 75 °C. The yield of pure compound **7b** as a white solid was 103 mg (56%); mp = 254−258 °C. UPLC (254 nm): 100 area %; MS (ESI): m/z = 245.2 (M + 2H$^+$)/2 calcd for free base 488.18. ^{1}H NMR (300 MHz, DMSO-d_6) (δ ppm): 10.58 (s, 4H, −C(NH−)$_2^+$), 8.69 (d, 2H, J = 1.6 Hz, Ar−H), 8.19 (d, 2H, J = 8.4 Hz, Ar−H), 8.00 (dd, 2H, J = 8.4 Hz, J = 1.6 Hz, Ar−H), 4.05 (s, 8H, −CH_2CH_2−), 3.20 (t, 4H, J = 7.4 Hz, −CH_2(CH$_2$)$_4$CH_2−), 2.35 (s, 6H, CH_3SO$_3^-$), 1.86 (br s, 4H, −CH$_2$CH_2(CH$_2$)$_2$CH_2CH$_2$−), 1.47 (br s, 4H, −(CH$_2$)$_2$(CH_2)$_2$(CH$_2$)$_2$−). ^{13}C NMR (75 MHz, D$_2$O) (δ ppm): 180.2 (s), 165.4 (s), 155.3 (s), 135.2 (s), 125.4 (d), 122.6 (d), 122.0 (d), 118.0 (s), 44.6 (t), 38.4 (q), 33.3 (t), 28.4 (t), 27.8 (t). Analysis calculated for C$_{28}$H$_{36}$N$_6$O$_6$S$_4$·3H$_2$O (734.93): C, 45.76; H, 5.76; N, 11.44. Found: C, 45.81; H, 5.65; N, 11.38.

*4.1.2.13. 2,2′-(Hexane-1,6-diyl)bis-6-(3,4,5,6-tetrahydropyrimidinium-2-yl)benzothiazole Dimethansulfonate (**7c**).* 2-Amino-5-(3,4,5,6-tetrahydropyrimidin-1-ium-2-yl)benzenethiolate (**1c**) (0.105 g, 0.5 mmol) and suberic acid (**2e**) (44 mg, 0.25 mmol) were heated in PPA (10.6 g). The crude free base was then dissolved in 2-PrOH (5 mL), and methanesulfonic acid (65 μL, 1.0 mmol) was added, stirred at room temperature for 1 h, and precipitated by the addition of diethyl ether. The resulting precipitate was filtered and dried at 75 °C. The yield of pure compound **7c** as a white hygroscopic solid was 139 mg (71%); mp = 258−264 °C. UPLC (230 nm): 100 area %; MS (ESI): m/z = 259.3 (M + 2H$^+$)/2 calcd for free base 516.21. ^{1}H NMR (600 MHz, DMSO-d_6) (δ ppm): 10.00 (s, 4H, −C(NH−)$_2^+$), 8.48 (s, 2H, Ar−H), 8.14 (d, 2H, J = 8.5 Hz, Ar−H), 7.78 (d, 2H, J = 8.5 Hz, Ar−H), 3.52 (br s, 8H, −C(NH$^+$CH_2)$_2$−), 3.19 (t, 4H, J = 7.3 Hz, −CH_2(CH$_2$)$_4$CH_2−), 2.31 (s, 6H, CH_3SO$_3^-$), 2.00 (m, 4H, −CH$_2$CH_2(CH$_2$)$_2$CH_2CH$_2$−), 1.86 (br s, 4H, −(CH$_2$)$_2$(CH_2)$_2$(CH$_2$)$_2$−) 1.47 (br s, 4H, −C(NH$^+$CH$_2$)$_2$CH_2). ^{13}C NMR (150 MHz, DMSO-d_6) (δ ppm): 176.3 (s), 159.1 (s), 155.5 (s), 135.0 (s), 125.3 (d), 124.9 (s), 122.4 (s), 39.7 (q), 38.9 (t), 33.5 (t), 28.5 (t), 28.0 (t), 17.7 (t). Analysis calculated for C$_{30}$H$_{40}$N$_6$O$_6$S$_4$·3H$_2$O (781.00): C, 46.14; H, 6.19; N, 10.76. Found: C, 46.02; H, 6.20; N, 10.80.

*4.1.2.14. 2,2′-(Heptane-1,7-diyl)bis-6-amidiniumbenzothiazole Dimethansulfonate (**8a**).* 2-Amino-5-amidiniumbenzenethiolate (**1a**) (84 mg, 0.5 mmol) and azelaic acid (**2f**) (47 mg, 0.25 mmol) were heated in PPA (9.8 g). The crude free base was then suspended in 2-PrOH (5 mL), and methanesulfonic acid (65 μL, 1.0 mmol) was added and stirred at room temperature for 1 h. After cooling overnight, the resulting precipitate was filtered, crystallized from the water/acetone mixture, and dried at 75 °C. Yield of pure compound **8a** as white solid was 63 mg (38%); mp = 226−232 °C. HPLC (220 nm): 96.0 area %; MS (ESI): m/z = 226.5 (M + 2H$^+$)/2 calcd for free base 450.17. ^{1}H NMR (300 MHz, DMSO-d_6) (δ ppm): 9.36 (br s, 4H, −C(NH_2)$_2^+$), 9.07 (br s, 4H, −C(NH_2)$_2^+$), 8.57 (d, 2H, J = 1.6 Hz, Ar−H), 8.14 (d, 2H, J = 8.8 Hz, Ar−H), 7.87 (dd, 2H, J = 8.8 Hz, J = 1.6 Hz, Ar−H), 3.19 (t, 4H, J = 7.5 Hz, −CH_2(CH$_2$)$_5$CH_2−), 2.35 (s, 6H, CH_3SO$_3^-$), 1.84 (m, 4H, −CH$_2$CH_2(CH$_2$)$_3$CH_2CH$_2$−), 1.41 (br s, 6H, −(CH$_2$)$_2$(CH_2)$_3$(CH$_2$)$_2$−). ^{13}C NMR (75 MHz, DMSO-d_6) (δ ppm): 176.7 (s), 165.4 (s), 155.9 (s), 134.9 (s), 125.8 (d), 124.4 (s), 123.1 (d), 122.3 (d), 39.7 (q), 33.5 (t), 28.7 (t), 28.2 (t). Analysis calculated for C$_{25}$H$_{34}$N$_6$O$_6$S$_4$·H$_2$O (660.85): C, 45.44; H, 5.49; N, 12.72. Found: C, 45.36; H, 5.82; N, 12.50.

*4.1.2.15. 2,2′-(Heptane-1,7-diyl)bis-6-(4,5-dihydro-1H-imidazolium-2-yl)benzothiazole Dimethansulfonate (**8b**).* 2-Amino-5-(4,5-dihydro-1H-imidazol-3-ium-2-yl)benzenethiolate hydrate (**1b**) (106 mg, 0.50 mmol) and azelaic acid (**2f**) (47 mg, 0.25 mmol) were heated in PPA (9.1 g). The resulting crude free base was dissolved in 2-PrOH (10 mL), and methanesulfonic acid (65 μL, 1.0 mmol) was added, stirred at room temperature for 1 h, and precipitated by the addition of diethyl ether. The resulting precipitate was filtered, crystallized from the water/acetone mixture, and dried at 75 °C. The yield of pure compound **8b** as a white solid was 57 mg (31%); mp = 167−172 °C. HPLC (220 nm): 99.0 area %; MS (ESI): m/z = 252.5 (M + 2H$^+$)/2 calcd for free base 502.20. ^{1}H NMR (300 MHz, DMSO-d_6) (δ ppm): 10.55 (br s, 4H, −C(NH−)$_2^+$), 8.68 (d, 2H, J = 1.7 Hz, Ar−H), 8.19 (d, 2H, J = 8.6 Hz, Ar−H), 7.98 (dd, 2H, J = 8.6 Hz, J = 1.7 Hz, Ar−H), 4.05 (s, 8H, −CH_2CH_2−), 3.19 (t, 4H, J = 7.4 Hz, −CH_2(CH$_2$)$_5$CH_2−), 2.32 (s, 6H, CH_3SO$_3^-$), 1.91−1.78 (m, 4H, −CH$_2$CH_2(CH$_2$)$_3$CH_2CH$_2$−), 1.41 (br s, 6H, −(CH$_2$)$_2$(CH_2)$_3$(CH$_2$)$_2$−). ^{13}C NMR (75 MHz, D$_2$O) (δ ppm): 180.3 (s), 165.2 (s), 155.3 (s), 135.2 (s), 125.3 (d), 122.5 (d), 122.0 (d), 117.9 (s), 44.6 (t), 38.4 (q), 33.3 (t), 28.4 (t), 27.7 (t). Analysis

https://doi.org/10.1021/acs.jmedchem.3c01051
J. Med. Chem. XXXX, XXX, XXX−XXX

calculated for $C_{29}H_{38}N_6O_6S_4{\cdot}2H_2O$ (730.94): C, 47.65; H, 5.79; N, 11.50. Found: C, 47.78; H, 5.58; N, 11.47.

*4.1.2.16. trans-2,2′-(Cyclohexane-1,4-diyl)bis-6-amidiniumbenzothiazole Dimethansulfonate (**9a**).* 2-Amino-5-amidiniumbenzenethiolate (**1a**) (168 mg, 1.0 mmol) and *trans*-1,4-cyclohexane dicarboxylic acid (**2g**) (86 mg, 0.5 mmol) were heated in PPA (14.0 g). The crude free base was then suspended in EtOH (20 mL), and methanesulfonic acid (130 μL, 2.0 mmol) was added and stirred at room temperature for 2 h. After cooling overnight, the resulting precipitate was filtered, crystallized from water, and dried at 75 °C. The yield of pure compound **9a** as a white solid was 172 mg (52%); mp > 300 °C. UPLC (230 nm): 99.6 area %; MS (ESI): m/z = 218.3 (M + 2H)/2 calcd for free base 434.13. ^{1}H NMR (300 MHz, DMSO-d_6) (δ ppm): 9.22 (br s, 8H, −C(NH_2)$_2^+$), 8.62 (d, 2H, J = 1.6 Hz, Ar−H), 8.18 (d, 2H, J = 8.6 Hz, Ar−H), 7.89 (dd, 2H, J = 8.6 Hz, J = 1.6 Hz, Ar−H), 2.43−2.29 (m, 10H, CHex−H + CH_3SO$_3^-$), 1.88 (m, 4H, CHex−H). ^{1}H NMR (300 MHz, D_2O) (δ ppm): 8.45 (d, 2H, J = 1.6 Hz, Ar−H), 8.10 (d, 2H, J = 8.6 Hz, Ar−H), 7.88 (dd, 2H, J = 8.6 Hz, J = 1.6 Hz, Ar−H), 3.24 (m, 2H, CHex−H), 2.81 (s, 6H, CH_3SO$_3^-$), 2.32 (m, 4H, CHex−H), 1.79 (m, 4H, CHex−H). ^{13}C NMR (150 MHz, DMSO-d_6) (δ ppm): 180.7 (s), 165.4 (s), 155.7 (s), 134.4 (s), 125.8 (d), 124.5 (s), 123.2 (d), 122.5 (d), 41.7 (d), 39.7 (q), 31.9 (t). Analysis calculated for $C_{24}H_{30}N_6O_6S_4{\cdot}2H_2O$ (662.82): C, 43.49; H, 5.17; N, 12.68. Found: C, 43.58; H, 5.03; N, 12.73.

*4.1.2.17. trans-2,2′-(Cyclohexane-1,4-diyl)bis-6-(4,5-dihydro-1H-imidazolium-2-yl)benzothiazole Dimethansulfonate (**9b**).* 2-Amino-5-(4,5-dihydro-1H-imidazol-3-ium-2-yl)benzenethiolate hydrate (**1b**) (212 mg, 1.0 mmol) and *trans*-1,4-cyclohexane dicarboxylic acid (**2g**) (86 mg, 0.5 mmol) were heated in PPA (13.0 g). The resulting crude free base was suspended in 2-PrOH (20 mL), and methanesulfonic acid (130 μL, 2.0 mmol) was added and stirred at room temperature for 4 h. After cooling overnight, the resulting precipitate was filtered, crystallized from EtOH, and dried at 75 °C. The yield of pure compound **9b** as a white solid was 222 mg (59%); mp > 300 °C. UPLC (254 nm): 100 area %; MS (ESI): m/z = 244.3 (M + 2H)/2 calcd for free base 486.17. ^{1}H NMR (300 MHz, DMSO-d_6) (δ ppm): 10.57 (s, 4H, −C(NH−)$_2^+$), 8.72 (d, 2H, J = 1.7 Hz, Ar−H), 8.24 (d, 2H, J = 8.6 Hz, Ar−H), 8.01 (dd, 2H, J = 8.6 Hz, J = 1.7 Hz, Ar−H), 4.06 (s, 8H, −CH_2CH_2−), 3.40 (m, 2H, CHex−H), 2.37 (m, 4H, CHex−H), 2.31 (s, 6H, CH_3SO$_3^-$), 1.89 (m, 4H, CHex−H). ^{1}H NMR (300 MHz, D_2O) (δ ppm): 8.43 (d, 2H, J = 1.6 Hz, Ar−H), 8.10 (d, 2H, J = 8.6 Hz, Ar−H), 7.84 (dd, 2H, J = 8.6 Hz, J = 1.6 Hz, Ar−H), 3.90 (s, 8H, −CH_2CH_2−), 2.80 (s, 6H, CH_3SO$_3^-$), 2.67 (m, 2H, CHex−H), 2.01 (m, 4H, CHex−H), 1.38 (m, 4H, CHex−H). ^{13}C NMR (75 MHz, D_2O) (δ ppm): 183.8 (s), 165.4 (s), 155.5 (s), 134.9 (s), 125.8 (d), 123.0 (d), 122.4 (d), 118.4 (s), 44.5 (t), 41.6 (d), 38.4 (q), 31.5 (t). Analysis calculated for $C_{28}H_{34}N_6O_6S_4{\cdot}4H_2O$ (750.93): C, 44.78; H, 5.64; N, 11.19. Found: C, 44.56; H, 5.82; N, 11.30.

*4.1.2.18. trans-2,2′-(Cyclohexane-1,4-diyl)bis-6-(3,4,5,6-tetrahydropyrimidinium-2-yl)benzothiazole Dimethansulfonate (**9c**).* 2-Amino-5-(3,4,5,6-tetrahydropyrimidin-1-ium-2-yl)benzenethiolate (**1c**) (0.214 g, 1.0 mmol) and *trans*-1,4-cyclohexane dicarboxylic acid (**2g**) (86 mg, 0.5 mmol) were heated in PPA (12.8 g). The crude free base was then suspended in 2-PrOH (10 mL), and methanesulfonic acid (130 μL, 2.0 mmol) was added and stirred at room temperature for 1 h. After cooling overnight, the resulting precipitate was filtered, crystallized from EtOH, and dried at 75 °C. The yield of pure compound **9c** as a white solid was 199 mg (55%); mp > 300 °C. UPLC (230 nm): 99.1 area %; MS (ESI): m/z = 258.3 (M + 2H)/2 calcd for free base 514.20. ^{1}H NMR (300 MHz, DMSO-d_6) (δ ppm): 10.01 (br s, 4H, −C(NH−)$_2^+$), 8.52(d, 2H, J = 1.6 Hz, Ar−H), 8.19 (d, 2H, J = 8.6 Hz, Ar−H), 7.80 (dd, 2H, J = 8.6 Hz, J = 1.6 Hz, Ar−H), 3.53 (t, 8H, J = 5.4 Hz, −C(NH$^+$CH_2)$_2$−), 3.37 (m, 2H, CHex−H), 2.36 (m, 4H, CHex−H), 2.30 (s, 6H, CH_3SO$_3^-$) 2.01 (m, 4H, −C(NH$^+$CH$_2$)$_2$CH_2), 1.88 (m, 4H, CHex−H). ^{13}C NMR (75 MHz, D_2O) (δ ppm): 182.9 (s), 159.6 (s), 154.8 (s), 134.7 (s), 125.2 (s), 125.1 (d), 122.3 (d), 121.8 (d), 41.6 (d), 39.1 (t), 38.4 (q), 31.6 (t), 17.5 (t). Analysis calculated for $C_{30}H_{38}N_6O_6S_4{\cdot}0.4C_2H_5OH$ (725.35): C, 51.00; H, 5.61; N, 11.59. Found: C, 51.04; H, 5.66; N, 11.57.

*4.1.2.19. trans-2,2′-(Ethene-1,2-diyl)bis-6-amidiniumbenzothiazole Dimethansulfonate (**10a**).* 2-Amino-5-amidiniumbenzenethiolate (**1a**) (168 mg, 1.0 mmol) and fumaric acid (**2h**) (58 mg, 0.5 mmol) were heated in PPA (12.0 g). The crude free base was then suspended in EtOH (10 mL), and methanesulfonic acid (130 μL, 2.0 mmol) was added and stirred at room temperature for 2 h. After cooling overnight, the resulting precipitate was filtered, crystallized from EtOH, and dried at 75 °C. The yield of pure compound **10a** as a pale yellow solid was 138 mg (45%); mp > 300 °C. UPLC (230 nm): 99.2 area %; MS (ESI): m/z = 379.1 (M + H$^+$) calcd for free base 378.07. ^{1}H NMR (300 MHz, DMSO-d_6) (δ ppm): 9.44 (br s, 4H, −C(NH_2)$_2^+$), 9.09 (br s, 4H, −C(NH_2)$_2^+$), 8.71(s, 2H, Ar−H), 8.31 (d, 2H, J = 8.3 Hz, Ar−H), 8.18 (s, 2H, −CH = CH−),7.94 (d, 2H, J = 8.3 Hz, Ar−H), 2.33 (s, 6H, CH_3SO$_3^-$). ^{13}C NMR (75 MHz, DMSO-d_6) (δ ppm): 168.1 (s), 165.3 (s), 156.2 (s), 135.3 (s), 129.9 (d), 126.6 (d), 125.7 (s), 123.6 (d), 123.4 (d). Analysis calculated for $C_{20}H_{22}N_6O_6S_4{\cdot}2H_2O$ (615.73): C, 39.59; H, 4.32; N, 13.85. Found: C, 39.72; H, 4.45; N, 13.78.

*4.1.2.20. trans-2,2′-(Ethene-1,2-diyl)bis-6-(4,5-dihydro-1H-imidazolium-2-yl)benzothiazole Dimethansulfonate (**10b**).* 2-Amino-5-(4,5-dihydro-1H-imidazol-3-ium-2-yl)benzenethiolate hydrate (**1b**) (106 mg, 0.50 mmol) and fumaric acid (**2h**) (29 mg, 0.25 mmol) were heated in PPA (12.6 g). The resulting crude free base was suspended in EtOH (10 mL), and methanesulfonic acid (65 μL, 1.0 mmol) was added and stirred at room temperature for 2 h. After cooling overnight, the resulting precipitate was filtered, crystallized from EtOH, and dried at 75 °C. The yield of pure compound **10b** as a yellow solid was 65 mg (39%); mp > 300 °C. UPLC (230 nm): 99.0 area %; MS (ESI): m/z = 431.6 (M + H$^+$) calcd for free base 430.10. ^{1}H NMR (300 MHz, DMSO-d_6) (δ ppm): 10.61 (s, 4H, −C(NH−)$_2^+$), 8.79 (d, 2H, J = 1.5 Hz, Ar−H), 8.36 (d, 2H, J = 8.5 Hz, Ar−H), 8.21 (s, 2H, −CH═CH−), 8.06 (dd, 2H, J = 8.5 Hz, J = 1.5 Hz, Ar−H), 4.07 (s, 8H, −CH_2CH_2−), 2,31 (s, 6H, CH_3SO$_3^-$). ^{13}C NMR (150 MHz, D_2O) (δ ppm): 166.1 (s), 160.5 (s), 152.3 (s), 132.4 (s), 125.0 (d), 122.7 (d), 120.6 (d), 120.1 (d), 115.2 (s), 41.7 (t), 35.8 (q). Analysis calculated for $C_{24}H_{26}N_6O_6S_4{\cdot}2.5H_2O$ (667.80): C, 43.18; H, 4.68; N, 12.59. Found: C, 43.20; H, 4.64; N, 12.63.

*4.1.2.21. trans-2,2′-(Ethene-1,2-diyl)bis-6-(3,4,5,6-tetrahydropyrimidinium-2-yl)benzothiazole Dimethansulfonate (**10c**).* 2-Amino-5-(3,4,5,6-tetrahydropyrimidin-1-ium-2-yl)benzenethiolate (**1c**) (0.210 g, 1.0 mmol) and fumaric acid (**2h**) (58 mg, 0.5 mmol) were heated in PPA (11.6 g). Afterward, the crude free base was dissolved in EtOH (10 mL), and methanesulfonic acid (130 μL, 2.0 mmol) was added, stirred at room temperature for 1 h, and precipitated by the addition of diethyl ether. The resulting precipitate was filtered and dried at 75 °C. The yield of pure compound **10c** as a pale yellow solid was 78 mg (24%); mp = 285−290 °C (dec.). UPLC (254 nm): 100 area %; MS (ESI): m/z = 230.2 (M + 2H$^+$)/2 calcd for free base 458.13. ^{1}H NMR (300 MHz, DMSO-d_6) (δ ppm): 10.07 (s, 4H, −C(NH−)$_2^+$), 8.61(d, 2H, J = 1.6 Hz, Ar−H), 8.31 (d, 2H, J = 8.6 Hz, Ar−H), 8.17 (s, 2H, −CH═CH−), 7.86 (dd, 2H, J = 8.6 Hz, J = 1.6 Hz, Ar−H), 3.55 (t, 8H, J = 5.1 Hz, −C(NH$^+$CH_2)$_2$−), 2.30 (s, 6H, CH_3SO$_3^-$) 2.02 (m, 4H, −C(NH$^+$CH$_2$)$_2$CH_2). ^{13}C NMR (75 MHz, D_2O) (δ ppm): 168.6 (s), 158.6 (s), 154.8 (s), 135.2 (s), 128.5 (d), 125.4 (s), 125.0 (d), 123.3 (d), 121.5 (d), 39.1 (t), 38.5 (q), 17.5 (t). Analysis calculated for $C_{26}H_{30}N_6O_6S_4$ (650.81): C, 47.98; H, 4.65; N, 12.91. Found: C, 48.03; H, 4.51; N, 12.91.

4.1.3. T. brucei In Vitro Compound Screening. In vitro growth inhibition studies were carried out using bloodstream form *T. b. brucei* variant 221a (MiTat1.2a) cultured at 37 °C in modified Iscove's medium, as previously described.[70] Assays were performed in 96-well microtiter plates (200 μL volumes), and each experiment was initiated at 2.5 × 10^4 parasites mL^{-1}, with test compounds added at a range of concentrations. Plates were incubated at 37 °C for 48 h, resazurin (20 μL at 0.125 mg mL^{-1}) was added, and the plates were then incubated for a further 16 h. Fluorescence intensities were determined using a BMG FLUOstar Omega plate reader (excitation 545 nm, emission

https://doi.org/10.1021/acs.jmedchem.3c01051
J. Med. Chem. XXXX, XXX, XXX−XXX

590 nm), and the data were analyzed using GraphPad Prism 9.0 software. The values were expressed as EC_{50} ± SD and are the average of three independent replicates. For cytotoxicity assays, the rat myoblast L6 line was seeded into 96-well microtiter plates at 1×10^4 mL^{-1} in 200 μL of RPMI-1640 growth medium, and different compound concentrations were added. The plates were incubated for 6 days at 37 °C and 20 μL of resazurin was then added to each well. After a further 6 h incubation, the fluorescence was determined by a plate reader, as outlined above. For the BafA1:**9a** co-treatment experiment (Figure 5A), bloodstream form *T. brucei* were pre-incubated for 6 h in 4 or 8 nM BafA1 before addition of compound **9a** and then incubated as above in the continued presence of BafA1.

4.1.4. In Silico ADME Profiling. Physico-chemical and ADME parameters were calculated by ACD Percepta 2021.1.3. software [Predict Molecular Properties|Percepta Software|ACD/Labs (https://www.acdlabs.com/)].

4.1.5. In Vitro ADME Profiling. 4.1.5.1. MDCKII-MDR1 Permeability Assay. MDCKII-hMDR1 cells were obtained from Solvo Biotechnology, Hungary. DMEM, fetal bovine serum, Glutamax-100, antibiotic/antimycotic, DMSO, Dulbecco's phosphate buffer saline, and MEM Non-essential amino acids were purchased from Sigma (St. Louis, MO, USA). Bi-directional permeability and *P*-glycoprotein substrate assessment were investigated in Madin−Darby canine epithelial cells with over-expressed human MDR1 gene (*MDCKII-MDR1*), coding for *P*-glycoprotein. Experimental procedures and cell culture conditions were as previously described.[47] Briefly, compounds (10 μM, 1% DMSO v/v) in duplicate were incubated at 37 °C for 60 min with cell monolayers on 24-well Millicell inserts (Millipore, Burlington, MA, USA) without and with the *P*-glycoprotein inhibitor Elacridar (2 μM, International Laboratory, USA). Inhibition of *P*-glycoprotein was verified by amprenavir (Moravek Biochemicals Inc., Brea, CA, USA) and monolayer integrity by Lucifer yellow (Sigma, St. Louis, MO, USA). Compound concentrations were measured by LC−MS/MS, and Lucifer yellow was measured on an Infinite F500 (Tecan, Männedorf, CH) using excitation of 485 nm and emission of 530 nm.

4.1.5.2. Metabolic Stability. Mouse liver microsomes were obtained from Corning Life Sciences (Corning, USA). DMSO, nicotinamide adenine dinucleotide phosphate (NADP), glucose-6-phosphate, glucose-6-phosphate dehydrogenase, magnesium chloride, propranolol, caffeine, diclofenac, and phosphate buffer saline (PBS) were purchased from Sigma (St. Louis, MO, USA). Acetonitrile (ACN) and methanol (MeOH) were obtained from Merck (Darmstadt, Germany). Testosterone was purchased from Steraloids (Newport, RI, USA). Metabolic stability was assessed in mouse liver microsomes. Compounds (final concentration of 1 μM, 0.03% DMSO v/v) were incubated in duplicate in phosphate buffer (50 mM, pH 7.4) at 37 °C together with mouse liver microsomes in the absence and presence of the NADPH cofactor (0.5 mM NADPH, 5 mM glucose-6-phosphate, 1.5 U mL^{-1} glucose-6-phosphate dehydrogenase, and 0.5 mM $MgCl_2$). Incubation and sampling were performed on a Freedom EVO 200 (Tecan, Männedorf, CH) at 0.3, 10, 20, 30, 45, and 60 min. The reaction was quenched using 3 volumes of a mixture of ACN/MeOH (2:1) containing an internal standard (diclofenac) and centrifuged, and the supernatants were analyzed using LC−MS/MS.

Metabolic activity of microsomes was verified by simultaneous analysis of several controls, including testosterone, propranolol, and caffeine. The in vitro half-life ($t_{1/2}$) was calculated using GraphPad Prism non-linear regression of % parent compound remaining versus time. In vitro clearance, expressed as μL min^{-1} mg^{-1}, was estimated from $t_{1/2}$ and normalized for the protein amount in the incubation mixture, assuming 52.5 mg of protein per gram of liver.

4.1.5.3. LC−MS/MS Analysis. All samples were quantified using tandem mass spectrometry coupled to liquid chromatography. Samples were analyzed on a Sciex API4000 Triple Quadrupole Mass Spectrometer (Sciex, Division of MDS Inc., Toronto, Canada) coupled to a Shimadzu Nexera X2 UHPLC frontend (Kyto, Japan). Samples were injected onto a UHPLC column (HALO2 C18, 2.1 × 20 mm, 2 μm or Luna Omega 1.6 μm Polar C18 100A, 30 × 2.1 mm) and eluted with a gradient at 50 °C. The mobile phase was composed of the acetonitrile/water mixture (9/1, with 0.1% formic acid) and 0.1% formic acid in deionized water. The flow rate was 0.7 mL min^{-1} and under gradient conditions, leading to a total run time of 1.5−2 min. Positive ion mode with turbo spray, an ion source temperature of 550 °C, and a dwell time of 150 ms were utilized for mass spectrometric detection. Quantitation was performed using multiple reaction monitoring at the specific transitions for each compound.

4.1.6. T. brucei In Vivo Screening. For in vivo screening, we used the pleomorphic *T. b. brucei* GVR35-VSL2 strain that expresses a red-shifted luciferase transgene (*PpyRE9h*).[48] The threshold of detection by in vivo imaging is <100 parasites. Infections, using BALB/c or CD1 mouse models as indicated, were initiated by i.p. inoculation with 30,000 bloodstream form parasites. Mice were maintained in individually ventilated cages under specific pathogen-free conditions with a 12 h light/dark cycle and given food and water ad libitum. Experiments were performed under UK Home Office project license P9AEE04E4 with the consent of the LSHTM Animal Welfare and Ethical Review Board (AWERB). All protocols and procedures were conducted in accordance with the UK Animals (Scientific Procedures) Act 1986 (ASPA). For in vivo bioluminescence imaging, mice were injected i.p. with 150 mg kg^{-1} d-luciferin in PBS and then anesthetized using 2.5% (v/v) gaseous isoflurane.[48] 5 min after d-luciferin administration, they were placed in a PerkinElmer IVIS Spectrum Imager, and images were acquired using LivingImage 4.7. Exposure times varied between 30 s and 5 min, depending on signal intensity. After imaging, mice were allowed to recover and returned to cages.

For ex vivo imaging, mice were injected i.p. with 150 mg kg^{-1} D-luciferin and then sacrificed by exsanguination under terminal anesthesia 5 min later.[71] Mice were perfused with 10 mL 0.3 mg mL^{-1} D-luciferin in PBS via the heart. Organs and tissues were removed, transferred to a Petri dish, arranged in a standardized format, soaked in 0.3 mg mL^{-1} D-luciferin, and then imaged, as mentioned above.

*4.1.6.1. Genetic Approaches Used to Investigate Compound **9a** Uptake by T. brucei.* The bloodstream form *T. brucei* MiTat 1.2, clone 221a RNAi library was maintained as described.[49,51] Following RNAi induction with tetracycline (1 μg mL^{-1}), the library was selected for 10 days in the presence of inhibitory concentrations of **9a** (1−2 ng mL^{-1}). The *Tbaqp* null mutant lines (provided by Prof. David Horn, University of Dundee) were generated as described previously.[49,50] EC_{50} values were determined in vitro using microtitre plate assays, as outlined above. Each cell line was tested in triplicate.

4.1.7. Fluorescence Microscopy. Images were acquired using an inverted Nikon Eclipse microscope. Slides containing the parasites were moved along the *x*−*y* plane through 580 nm LED illumination. Images were collected using a 16 bit, 1-megapixel Pike AVT (F-100B) CCD camera set in the detector plane. An Nikon 60×/1.40 objective was used to collect the exit wave leaving the specimen. For co-localization assays, parasites were pre-incubated with 100 nM LysoTracker (Invitrogen) for 45 min and then washed in pre-warmed medium to remove the non-internalized dye prior to the addition of compound **9a** (10 μg mL^{-1}). For each timepoint studied, an aliquot of parasites was fixed in 4% PFA (paraformaldehyde) and mounted using VECTASHIELD Antifade Mounting Media with DAPI (for nuclear staining). For *Tb*CatL co-localization immunofluorescence microscopy, parasites were fixed with 4% PFA for 20 min, permeabilized with 0.1% Triton X-100 for 3 min, and blocked with 1% BSA for 1 h. Then, parasites were incubated overnight at 4 °C with an immunostaining solution containing 1:200 rabbit anti-*Tb*CatL (a gift from Prof. James Bangs, University of Buffalo). After washing, parasites were incubated for 1 h at 37 °C with 2 μg mL^{-1} goat anti-rabbit IgG secondary antibody, Alexa FluorTM 488. Finally, parasites were mounted as above.

4.1.8. P. falciparum Screening Assay. *P. falciparum* 3D7 strain asexual parasites were cultured in human erythrocytes (NHS Blood and Transfusion Service, UK) in RPMI 1640 medium supplemented with 0.5% Albumax II, 50 μM hypoxanthine, and 2 mM L-glutamine under a 5% CO_2 environment. The asexual growth assay was

https://doi.org/10.1021/acs.jmedchem.3c01051
J. Med. Chem. XXXX, XXX, XXX−XXX

performed as described,[72] with minor modifications. Briefly, 96-well flat-bottomed plates were prepared with appropriate compound **9a** dilutions dissolved in DMSO. 100 μL parasite aliquots, diluted to 2% parasitemia/1% hematocrit, were dispensed into each well, and plates were incubated for 96 h at 37 °C. Plates were frozen at −20 °C overnight to aid cell lysis. They were then thawed, and 100 μL of lysis solution (20 mM Tris pH 7.5, 5 mM EDTA, 0.008% w/vol Saponin, 0.08% wt/vol Triton X-100, and 1:5000 SYBR green) was added to each well and mixed thoroughly. After 1 h, plates were read using a fluorescence plate reader (excitation 485 nm, emission 535 nm). Fluorescence intensity was normalized to controls consisting of DMSO (solvent control) and 1 μM dihydroartemisinin (positive control) and expressed as percentage inhibition. Triplicate independent experiments were performed, and dose response curves and EC_{50} values were calculated using GraphPad Prism 9.0 software.

■ ASSOCIATED CONTENT

Supporting Information

The Supporting Information is available free of charge at https://pubs.acs.org/doi/10.1021/acs.jmedchem.3c01051.

Efficacy of compound **9a** against stage 2 African trypanosomiasis in mice; channel protein aquaglyceroporin-2 (TbAQP-2) is not a major mediator of compound **9a** uptake by bloodstream form *T. brucei*; ^{1}H and ^{13}C NMR spectra of novel compounds **3a−10c**; UPLC-MS spectra of compound **9a**; and representative HPLC traces (PDF)

Smiles Molecular Formulae (CSV)

■ AUTHOR INFORMATION

Corresponding Authors

Livio Racané − *Department of Applied Chemistry, Faculty of Textile Technology, University of Zagreb, 10000 Zagreb, Croatia*; Email: livio.racane@ttf.unizg.hr

John M. Kelly − *Department of Infection Biology, London School of Hygiene and Tropical Medicine, WC1E 7HT London, U.K.*; orcid.org/0000-0003-4305-5258; Email: john.kelly@lshtm.ac.uk

Authors

Lucija Ptiček − *Department of Applied Chemistry, Faculty of Textile Technology, University of Zagreb, 10000 Zagreb, Croatia*

Sanja Kostrun − *Chemistry Department, Selvita Ltd., 10000 Zagreb, Croatia*

Silvana Raić-Malić − *Department of Organic Chemistry, Faculty of Chemical Engineering and Technology, University of Zagreb, 10000 Zagreb, Croatia*

Martin Craig Taylor − *Department of Infection Biology, London School of Hygiene and Tropical Medicine, WC1E 7HT London, U.K.*; orcid.org/0000-0003-4147-0693

Michael Delves − *Department of Infection Biology, London School of Hygiene and Tropical Medicine, WC1E 7HT London, U.K.*; orcid.org/0000-0001-8526-4782

Sam Alsford − *Department of Infection Biology, London School of Hygiene and Tropical Medicine, WC1E 7HT London, U.K.*

Francisco Olmo − *Department of Infection Biology, London School of Hygiene and Tropical Medicine, WC1E 7HT London, U.K.*

Amanda Fortes Francisco − *Department of Infection Biology, London School of Hygiene and Tropical Medicine, WC1E 7HT London, U.K.*

Complete contact information is available at: https://pubs.acs.org/10.1021/acs.jmedchem.3c01051

Author Contributions

The manuscript was written through the contributions of all authors. All authors have given approval to the final version of the manuscript.

Notes

The authors declare no competing financial interest.

■ ACKNOWLEDGMENTS

We greatly appreciate the financial support of the Croatian Science Foundation (projects no. IP-2018-01-4379 and IP-2018-01-4682) and the UK Medical Research Council (MRC) (grant MR/T015969/1).

■ ABBREVIATIONS

AB, apical−basolateral; BA, basolateral−apical; BafA1, bafilomycin A1; kDNA, kinetoplast DNA; LBF, liver blood flow; P_{app}, apparent permeability; Pe (Caco-2), Caco-2 cell permeability; RIT-seq, RNAi target sequencing; SI, selectivity index; V-type ATPase, vacuolar-type proton ATPase

■ REFERENCES

(1) World Health Organization. *Trypanosomiasis, Human African (Sleeping Sickness)*, 2022. https://www.who.int/news-room/fact-sheets/detail/trypanosomiasis-human-african-(sleeping-sickness).

(2) Yaro, M.; Munyard, K. A.; Stear, M. J.; Groth, D. M. Combatting African animal trypanosomiasis (AAT) in livestock: The potential role of trypanotolerance. *Vet. Parasitol.* **2016**, *225*, 43−52.

(3) Tanowitz, H. B.; Scherer, P. E.; Mota, M. M.; Figueiredo, L. M. Adipose tissue: A safe haven for parasites? *Trends Parasitol.* **2017**, *33*, 276−284.

(4) Crilly, N. P.; Mugnier, M. R. Thinking outside the blood: Perspectives on tissue-resident Trypanosoma brucei. *PLoS Pathog.* **2021**, *17*, No. e1009866.

(5) Kasozi, K. I.; MacLeod, E. T.; Ntulume, I.; Welburn, S. C. An update on African trypanocide pharmaceutics and resistance. *Front. Vet. Sci.* **2022**, *9*, 828111.

(6) Paine, M. F.; Wang, M. Z.; Generaux, C. N.; Boykin, D. W.; Wilson, W. D.; De Koning, H. P.; Olson, C. A.; Pohlig, G.; Burri, C.; Brun, R.; Murilla, G. A.; Thuita, J. K.; Barrett, M. P.; Tidwell, R. R. Diamidines for human African trypanosomiasis. *Curr. Opin. Invest. Drugs* **2010**, *11*, 876−883.

(7) Fairlamb, A. H.; Horn, D. Melarsoprol resistance in African trypanosomiasis. *Trends Parasitol.* **2018**, *34*, 481−492.

(8) Lutje, V.; Probyn, K.; Seixas, J.; Bergman, H.; Villanueva, G. Chemotherapy for second-stage human African trypanosomiasis: drugs in use. *Cochrane Database Syst. Rev.* **2012**, *2021*, CD015374.

(9) Mesu, V. K. B. K.; Kalonji, W. M.; Bardonneau, C.; Mordt, O. V.; Blesson, S.; Simon, F.; Delhomme, S.; Bernhard, S.; Kuziena, W.; Lubaki, J. P. F.; Vuvu, S. L.; Ngima, P. N.; Mbembo, H. M.; Ilunga, M.; Bonama, A. K.; Heradi, J. A.; Solomo, J. L. L.; Mandula, G.; Badibabi, L. K.; Dama, F. R.; Lukula, P. K.; Tete, D. N.; Lumbala, C.; Scherrer, B.; Strub-Wourgaft, N.; Tarral, A. Oral fexinidazole for late-stage African Trypanosoma brucei gambiense trypanosomiasis: a pivotal multicentre, randomised, non-inferiority trial. *Lancet* **2018**, *391*, 144−154.

(10) Lindner, A. K.; Lejon, V.; Chappuis, F.; Seixas, J.; Kazumba, L.; Barrett, M. P.; Mwamba, E.; Erphas, O.; Akl, E. A.; Villanueva, G.; Bergman, H.; Simarro, P.; Kadima Ebeja, A.; Priotto, G.; Franco, J. R. New WHO guidelines for treatment of gambiense human African trypanosomiasis including fexinidazole: substantial changes for clinical practice. *Lancet Infect. Dis.* **2020**, *20*, e38−e46.

(11) Giordani, F.; Morrison, L. J.; Rowan, T. G.; DE Koning, H. P.; Barrett, M. P. The animal trypanosomiases and their chemotherapy: a review. *Parasitol* **2016**, *143*, 1862−1889.
(12) Okello, I.; Mafie, E.; Eastwood, G.; Nzalawahe, J.; Mboera, L. E. G. African animal trypanosomiasis: A systematic review on prevalence, risk factors and drug resistance in sub-Saharan Africa. *J. Med. Entomol.* **2022**, *59*, 1099−1143.
(13) Vázquez-Jiménez, L. K.; Moreno-Herrera, A.; Juárez-Saldivar, A.; González-González, A.; Ortiz-Pérez, E.; Paz-González, A. D.; Palos, I.; Ramírez-Moreno, E.; Rivera, G. Recent advances in the development of triose phosphate isomerase inhibitors as antiprotozoal agents. *Curr. Med. Chem.* **2022**, *29*, 2504−2529.
(14) Melchor Doncel de la Torre, S.; Vázquez, C.; González-Chávez, Z.; Yépez-Mulia, L.; Nieto-Meneses, R.; Jasso-Chávez, R.; Saavedra, E.; Hernández-Luis, F. Synthesis and biological evaluation of 2-methyl-1H-benzimidazole-5-carbohydrazides derivatives as modifiers of redox homeostasis of Trypanosoma cruzi. *Bioorg. Med. Chem. Lett.* **2017**, *27*, 3403−3407.
(15) Pauli, I.; Ferreira, L. G.; de Souza, M. L.; Oliva, G.; Ferreira, R. S.; Dessoy, M. A.; Slafer, B. W.; Dias, L. C.; Andricopulo, A. D. Molecular modeling and structure activity relationships for a series of benzimidazole derivatives as cruzain inhibitors. *Future Med. Chem.* **2017**, *9*, 641−657.
(16) Velázquez-López, J. M.; Hernández-Campos, A.; Yépez-Mulia, L.; Téllez-Valencia, A.; Flores-Carrillo, P.; Nieto-Meneses, R.; Castillo, R. Synthesis and trypanocidal activity of novel benzimidazole derivatives. *Bioorg. Med. Chem. Lett.* **2016**, *26*, 4377−4381.
(17) Boiani, M.; Boiani, L.; Merlino, A.; Hernández, P.; Chidichimo, A.; Cazzulo, J. J.; Cerecetto, H.; González, M. Second generation of 2H-benzimidazole 1, 3-dioxide derivatives as anti-trypanosomatid agents: synthesis, biologicalevaluation, and mode of action studies. *Eur. J. Med. Chem.* **2009**, *44*, 4426−4433.
(18) Doganc, F.; Celik, I.; Eren, G.; Kaiser, M.; Brun, R.; Goker, H. Synthesis, in vitro antiprotozoal activity, molecular docking and molecular dynamics studies of some new monocationic guanidino-benzimidazoles. *Eur. J. Med. Chem.* **2021**, *221*, 113545.
(19) Moreno-Herrera, A.; Cortez-Maya, S.; Bocanegra-Garcia, V.; Banik, B. K.; Rivera, G. Recent advances in the development of broad-spectrum antiprotozoal agents. *Curr. Med. Chem.* **2021**, *28*, 583−606.
(20) Cuevas-Hernández, R. I.; Girard, R. M. B. M.; Krstulović, L.; Bajić, M.; Silber, A. M. An aromatic imidazoline derived from chloroquinoline triggers cell cycle arrest and inhibits with high selectivity the Trypanosoma cruzi mammalian host-cells infection. *PLoS Neglected Trop. Dis.* **2021**, *15*, No. e0009994.
(21) Karaaslan, C.; Kaiser, M.; Brun, R.; Göker, H. Synthesis and potent antiprotozoal activity of mono/di amidino 2-anilinobenzimidazoles versus Plasmodium falciparum and Trypanosoma brucei rhodesiense. *Bioorg. Med. Chem.* **2016**, *24*, 4038−4044.
(22) Farahat, A. A.; Bennett-Vaughn, C.; Mineva, E. M.; Kumar, A.; Wenzler, T.; Brun, R.; Liu, Y.; Wilson, W. D.; Boykin, D. W. Synthesis, DNA binding and antitrypanosomal activity of benzimidazole analogues of DAPI. *Bioorg. Med. Chem. Lett.* **2016**, *26*, 5907−5910.
(23) Ismail, M. A.; Batista-Parra, A.; Miao, Y.; Wilson, W. D.; Wenzler, T.; Brun, R.; Boykin, D. W. Dicationic near-linear biphenyl benzimidazole derivatives as DNA-targeted antiprotozoal agents. *Bioorg. Med. Chem.* **2005**, *13*, 6718−6726.
(24) Mathis, A. M.; Bridges, A. S.; Ismail, M. A.; Kumar, A.; Francesconi, I.; Anbazhagan, M.; Hu, Q.; Tanious, F. A.; Wenzler, T.; Saulter, J.; Wilson, W. D.; Brun, R.; Boykin, D. W.; Tidwell, R. R.; Hall, J. E. Diphenyl furans and aza analogs: effects of structural modification on in vitro activity, DNA binding, and accumulation and distribution in trypanosomes. *Antimicrob. Agents Chemother.* **2007**, *51*, 2801−2810.
(25) Ward, C. P.; Wong, P. E.; Burchmore, R. J.; de Koning, H. P.; Barrett, M. P. Trypanocidal furamidine analogues: influence of pyridine nitrogens on trypanocidal activity, transport kinetics, and resistance patterns. *Antimicrob. Agents Chemother.* **2011**, *55*, 2352−2361.
(26) McNamara, N.; Rahmani, R.; Sykes, M. L.; Avery, V. M.; Baell, J. Hit-to-lead optimization of novel benzimidazole phenylacetamides as broad spectrum trypanosomacides. *RSC Med. Chem.* **2020**, *11*, 685−695.
(27) Beltran-Hortelano, I.; Atherton, R. L.; Rubio-Hernández, M.; Sanz-Serrano, J.; Alcolea, V.; Kelly, J. M.; Pérez-Silanes, S.; Olmo, F. Design and synthesis of Mannich base-type derivatives containing imidazole and benzimidazole as lead compounds for drug discovery in Chagas Disease. *Eur. J. Med. Chem.* **2021**, *223*, 113646.
(28) López-Lira, C.; Tapia, R. A.; Herrera, A.; Lapier, M.; Maya, J. D.; Soto-Delgado, J.; Oliver, A. G.; Graham Lappin, A.; Uriarte, E. New benzimidazolequinones as trypanosomicidal agents. *Bioorg. Chem.* **2021**, *111*, 104823.
(29) Martínez-Cerón, S.; Gutiérrez-Nágera, N. A.; Mirzaeicheshmeh, E.; Cuevas-Hernández, R. I.; Trujillo-Ferrara, J. G. Phenylbenzothiazole derivatives: effects against a Trypanosoma cruzi infection and toxicological profiles. *Parasitol. Res.* **2021**, *120*, 2905−2918.
(30) Cuevas-Hernández, R. I.; Girard, R. M. B. M.; Martínez-Cerón, S.; Santos da Silva, M.; Elias, M. C.; Crispim, M.; Trujillo-Ferrara, J. G.; Silber, A. M. A fluorinated phenylbenzothiazole arrests the Trypanosoma cruzi cell cycle and diminishes the infection of mammalian host cells. *Antimicrob. Agents Chemother.* **2020**, *64*, 01742−1819.
(31) Linciano, P.; Pozzi, C.; Iacono, L. D.; di Pisa, F.; Landi, G.; Bonucci, A.; Gul, S.; Kuzikov, M.; Ellinger, B.; Witt, G.; Santarem, N.; Baptista, C.; Franco, C.; Moraes, C. B.; Müller, W.; Wittig, U.; Luciani, R.; Sesenna, A.; Quotadamo, A.; Ferrari, S.; Pöhner, I.; Cordeiro-da-Silva, A.; Mangani, S.; Costantino, L.; Costi, M. P. Enhancement of benzothiazoles as pteridine reductase-1 inhibitors for the treatment of trypanosomatidic infections. *J. Med. Chem.* **2019**, *62*, 3989−4012.
(32) Avila-Sorrosa, A.; Tapia-Alvarado, J. D.; Nogueda-Torres, B.; Chacón-Vargas, K. F.; Díaz-Cedillo, F.; Vargas-Díaz, M. E.; Morales-Morales, D. Facile synthesis of a series of non-symmetric thioethers including a benzothiazole moiety and their use as efficient in vitro anti-Trypanosoma cruzi agents. *Molecules* **2019**, *24*, 3077.
(33) Fleau, C.; Padilla, A.; Miguel-Siles, J.; Quesada-Campos, M. T.; Saiz-Nicolas, I.; Cotillo, I.; Cantizani Perez, J.; Tarleton, R. L.; Marco, M.; Courtemanche, G. Chagas disease drug discovery: multiparametric lead optimization against Trypanosoma cruzi in acylaminobenzothiazole series. *J. Med. Chem.* **2019**, *62*, 10362−10375.
(34) Racané, L.; Rep, V.; Kraljević Pavelić, S.; Grbčić, P.; Zonjić, I.; Radić Stojković, M.; Taylor, M. C.; Kelly, J. M.; Raić-Malić, S. Synthesis, antiproliferative and antitrypanosomal activities, and DNA binding of novel 6-amidino-2-arylbenzothiazoles. *J. Enzyme Inhib. Med. Chem.* **2021**, *36*, 1952−1967.
(35) Popov, A. B.; Krstulović, L.; Koštrun, S.; Jelić, D.; Bokulić, A.; Stojković, M. R.; Zonjić, I.; Taylor, M. C.; Kelly, J. M.; Bajić, M.; Raić-Malić, S. Design, synthesis, antitrypanosomal activity, DNA/RNA binding and in vitro ADME profiling of novel imidazoline-substituted 2-arylbenzimidazoles. *Eur. J. Med. Chem.* **2020**, *207*, 112802.
(36) Popov, A. B.; Stolić, I.; Krstulović, L.; Taylor, M. C.; Kelly, J. M.; Tomić, S.; Tumir, L.; Bajić, M.; Raić-Malić, S. Novel symmetric bis-benzimidazoles: Synthesis, DNA/RNA binding and antitrypanosomal activity. *Eur. J. Med. Chem.* **2019**, *173*, 63−75.
(37) Bistrović, A.; Krstulović, L.; Stolić, I.; Drenjančević, D.; Talapko, J.; Taylor, M. C.; Kelly, J. M.; Bajić, M.; Raić-Malić, S. Synthesis, anti-bacterial and anti-protozoal activities of amidinobenzimidazole derivatives and their interactions with DNA and RNA. *J. Enzyme Inhib. Med. Chem.* **2018**, *33*, 1323−1334.
(38) Racané, L.; Ptiček, L.; Sedić, M.; Grbčić, P.; Kraljević Pavelić, S.; Bertoša, B.; Sović, I.; Karminski-Zamola, G. Eco-friendly synthesis, in vitro anti-proliferative evaluation, and 3D-QSAR analysis of a novel series of monocationic 2-aryl/heteroaryl-substituted 6-(2-imidazolinyl)benzothiazole mesylates. *Mol. Diversity* **2018**, *22*, 723−741.
(39) Racané, L.; Kraljević Pavelić, S.; Ratkaj, I.; Stepanić, V.; Pavelić, K.; Tralić-Kulenović, V.; Karminski-Zamola, G. Synthesis and

https://doi.org/10.1021/acs.jmedchem.3c01051
J. Med. Chem. XXXX, XXX, XXX−XXX

antiproliferative evaluation of some new amidino-substituted bis-benzothiazolyl-pyridines and pyrazine. *Eur. J. Med. Chem.* **2012**, *55*, 108−116.
(40) Racané, L.; Pavelić, S. K.; Nhili, R.; Depauw, S.; Paul-Constant, C.; Ratkaj, I.; David-Cordonnier, M.-H.; Pavelić, K.; Tralić-Kulenović, V.; Karminski-Zamola, G. New anticancer active and selective phenylene-bisbenzothiazoles: Synthesis, antiproliferative evaluation and DNA Binding. *Eur. J. Med. Chem.* **2013**, *63*, 882−891.
(41) García-Báez, E. V.; Padilla-Martínez, I. I.; Tamay-Cach, F.; Cruz, A. Benzothiazoles from condensation of O-aminothiophenoles with carboxylic acids and their derivatives: A review. *Molecules* **2021**, *26*, 6518.
(42) Racané, L.; Tralić-Kulenović, V.; Mihalić, Z.; Pavlović, G.; Karminski-Zamola, G. Synthesis of new amidino-substituted 2-aminothiophenoles: mild basic ring opening of benzothiazole. *Tetrahedron* **2008**, *64*, 11594−11602.
(43) Racané, L.; Cindrić, M.; Zlatar, I.; Kezele, T.; Milić, A.; Brajša, K.; Hranjec, M. Preclinical in vitro screening of newly synthesised amidino substituted benzimidazoles and benzothiazoles. *J. Enzyme Inhib. Med. Chem.* **2021**, *36*, 163−174.
(44) Racané, L.; Stojković, R.; Tralić-Kulenović, V.; Cerić, H.; Đaković, M.; Ester, K.; Krpan, A. M.; Stojković, M. R. Interactions with polynucleotides and antitumor activity of amidino and imidazolinyl substituted 2-phenylbenzothiazole mesylates. *Eur. J. Med. Chem.* **2014**, *86*, 406−419.
(45) Lee, K.-J.; Johnson, N.; Castelo, J.; Sinko, P. J.; Grass, G.; Holme, K.; Lee, Y.-H. Effect of experimental pH on the in vitro permeability in intact rabbit intestines and Caco-2 monolayer. *Eur. J. Pharm. Sci.* **2005**, *25*, 193−200.
(46) Roy, H.; Nandi, S. In-silico modeling in drug metabolism and interaction: Current strategies of lead discovery. *Curr. Pharm. Des.* **2019**, *25*, 3292−3305.
(47) Acharya, P.; O'Connor, M. P.; Polli, J. W.; Ayrton, A.; Ellens, H.; Bentz, J. Kinetic identification of membrane transporters that assist P-glycoprotein-mediated transport of digoxin and loperamide through a confluent monolayer of MDCKII-hMDR1 cells. *Drug Metab. Dispos.* **2008**, *36*, 452−460.
(48) McLatchie, A. P.; Burrell-Saward, H.; Myburgh, E.; Lewis, M. D.; Ward, T. H.; Mottram, J. C.; Croft, S. L.; Kelly, J. M.; Taylor, M. C. Highly sensitive in vivo imaging of Trypanosoma brucei expressing "red-shifted" luciferase. *PLoS Neglected Trop. Dis.* **2013**, *7*, No. e2571.
(49) Alsford, S.; Eckert, S.; Baker, N.; Glover, L.; Sanchez-Flores, A.; Leung, K. F.; Turner, D. J.; Field, M. C.; Berriman, M.; Horn, D. High-throughput decoding of antitrypanosomal drug efficacy and resistance. *Nature* **2012**, *482*, 232−236.
(50) Baker, N.; Glover, L.; Munday, J. C.; Aguinaga Andrés, D.; Barrett, M. P.; de Koning, H. P.; Horn, D. Aquaglyceroporin 2 controls susceptibility to melarsoprol and pentamidine in African trypanosomes. *Proc. Natl. Acad. Sci. U.S.A.* **2012**, *109*, 10996−11001.
(51) Alsford, S.; Turner, D. J.; Obado, S. O.; Sanchez-Flores, A.; Glover, L.; Berriman, M.; Hertz-Fowler, C.; Horn, D. High-throughput phenotyping using parallel sequencing of RNA interference targets in the African trypanosome. *Genome Res.* **2011**, *21*, 915−924.
(52) Alsford, S.; Kelly, J. M.; Baker, N.; Horn, D. Genetic dissection of drug resistance in trypanosomes. *Parasitology* **2013**, *140*, 1478−1491.
(53) Alsford, S.; Field, M. C.; Horn, D. Receptor-mediated endocytosis for drug delivery in African trypanosomes: fulfilling Paul Ehrlich's vision of chemotherapy. *Trends Parasitol.* **2013**, *29*, 207−212.
(54) Link, F.; Borges, A. R.; Jones, N. G.; Engstler, M. To the surface and back: Exo- and endocytic pathways in Trypanosoma brucei. *Front. Cell Dev. Biol.* **2021**, *9*, 720521.
(55) Bowman, E. J.; Siebers, A.; Altendorf, K. Bafilomycins: a class of inhibitors of membrane ATPases from microorganisms, animal cells, and plant cells. *Proc. Natl. Acad. Sci. U.S.A.* **1988**, *85*, 7972−7976.
(56) Koeller, C. M.; Bangs, J. D. Processing and targeting of cathepsin L (TbCatL) to the lysosome in Trypanosoma brucei. *Cell. Microbiol.* **2019**, *21*, No. e12980.
(57) Bray, P. G.; Barrett, M. P.; Ward, S. A.; de Koning, H. P. Pentamidine uptake and resistance in pathogenic protozoa: past, present and future. *Trends Parasitol.* **2003**, *19*, 232−239.
(58) World Health Organization. *Interim Guidelines for the Treatment of Gambiense Human African Trypanosomiasis*; World Health Organization: Geneva, 2019. Licence: CC BY-NC-SA 3.0 IGO.
(59) P De Koning, H. The drugs of sleeping sickness: their mechanisms of action and resistance, and a brief history. *Trop. Med. Infect. Dis.* **2020**, *5*, 14.
(60) Stewart, M. L.; Krishna, S.; Burchmore, R. J. S.; Brun, R.; De Koning, H. P.; Boykin, D. W.; Tidwell, R. R.; Ed Hall, J.; Barrett, M. P. Detection of arsenical drug resistance in Trypanosoma brucei using a simple fluorescence test. *Lancet* **2005**, *366*, 486−487.
(61) Pardridge, W. M. Drug transport across the blood−brain barrier. *J. Cereb. Blood Flow Metab.* **2012**, *32*, 1959−1972.
(62) Engstler, M.; Thilo, L.; Weise, F.; Grünfelder, C. G.; Schwarz, H.; Boshart, M.; Overath, P. Kinetics of endocytosis and recycling of the GPI-anchored variant surface glycoprotein in Trypanosoma brucei. *J. Cell Sci.* **2004**, *117*, 1105−1115.
(63) Demmel, L.; Schmidt, K.; Lucast, L.; Havlicek, K.; Zankel, A.; Koestler, T.; Reithofer, V.; de Camilli, P.; Warren, G. The endocytic activity of the flagellar pocket in Trypanosoma brucei is regulated by an adjacent phosphatidylinositol phosphate kinase. *J. Cell Sci.* **2014**, *127*, 2351−2364.
(64) Xu, J.; Feng, H. T.; Wang, C.; Yip, K. H. M.; Pavlos, N.; Papadimitriou, J. M.; Wood, D.; Zheng, M. H. Effects of bafilomycin A1: An inhibitor of vacuolar H(+)-ATPases on endocytosis and apoptosis in RAW cells and RAW cell-derived osteoclasts. *J. Cell. Biochem.* **2003**, *88*, 1256−1264.
(65) Bayer, N.; Schober, D.; Prchla, E.; Murphy, R. F.; Blaas, D.; Fuchs, R. Effect of bafilomycin A1 and nocodazole on endocytic transport in HeLa Cells: Implications for viral uncoating and infection. *J. Virol.* **1998**, *72*, 9645−9655.
(66) Teplova, V. V.; Tonshin, A. A.; Grigoriev, P. A.; Saris, N. E.; Salkinoja-Salonen, M. S. Bafilomycin A1 is a potassium ionophore that impairs mitochondrial functions. *J. Bioenerg. Biomembr.* **2007**, *39*, 321−329.
(67) Saris, N. E.; Andersson, M. A.; Mikkola, R.; Andersson, L. C.; Teplova, V. V.; Grigoriev, P. A.; Salkinoja-Salonen, M. S. Microbial toxin's effect on mitochondrial survival by increasing K+ uptake. *Toxicol. Ind. Health* **2009**, *25*, 441−446.
(68) Dickie, E. A.; Giordani, F.; Gould, M. K.; Mäser, P.; Burri, C.; Mottram, J. C.; Rao, S. P. S.; Barrett, M. P. New drugs for human African trypanosomiasis: A twenty first century success story. *Trop. Med. Infect. Dis.* **2020**, *5*, 29.
(69) Counihan, N. A.; Modak, J. K.; de Koning-Ward, T. F. How malaria parasites acquire nutrients from their host. *Front. Cell Dev. Biol.* **2021**, *9*, 649184.
(70) Taylor, M. C.; McLatchie, A.; Kelly, J. M. Evidence that transport of iron from the lysosome to the cytosol in African trypanosomes is mediated by a mucolipin orthologue. *Mol. Microbiol.* **2013**, *89*, 420−432.
(71) Lewis, M. D.; Fortes Francisco, A.; Taylor, M. C.; Burrell-Saward, H.; McLatchie, A. P.; Miles, M. A.; Kelly, J. M. Bioluminescence imaging of chronic Trypanosoma cruzi infections reveals tissue-specific parasite dynamics and heart disease in the absence of locally persistent infection. *Cell. Microbiol.* **2014**, *16*, 1285−1300.
(72) van Schalkwyk, D. A.; Burrow, R.; Henriques, G.; Gadalla, N. B.; Beshir, K. B.; Hasford, C.; Wright, S. G.; Ding, X. C.; Chiodini, P. L.; Sutherland, C. J. Culture-adapted Plasmodium falciparum isolates from UK travellers: in vitro drug sensitivity, clonality and drug resistance markers. *Malar. J.* **2013**, *12*, 320.

https://doi.org/10.1021/acs.jmedchem.3c01051
J. Med. Chem. XXXX, XXX, XXX−XXX